C.P. No. 1242

C.P. No. 1242

PROCUREMENT EXECUTIVE, MINISTRY OF DEFENCE

AERONAUTICAL RESEARCH COUNCIL

CURRENT PAPERS

Measurement of the Internal Performance of a Rectangular Air Intake having Variable Geometry Compression Surfaces at Mach Numbers from 1.7 to 2.5

Part 11 The Effect of Incidence

by

C. S. Brown and E. L. Goldsmith

Aerodynamics Dept., R.A.E., Bedford

LONDON: HER MAJESTY'S STATIONERY OFFICE

1973

PRICE £1·20 NET

UDC 533.697.2 : 533.6.015 : 533.6.011.5

CP No.1242*
December 1971

MEASUREMENT OF THE INTERNAL PERFORMANCE OF A RECTANGULAR AIR INTAKE HAVING VARIABLE GEOMETRY COMPRESSION SURFACES AT MACH NUMBERS FROM 1.7 TO 2.5

Part II - The effect of incidence

by

C. S. Brown

E. L. Goldsmith

SUMMARY

Measurements have been made of the internal performance of a rectangular intake having variable geometry compression surfaces. The measurements have been made within a range of Mach numbers from 1.7 to 2.46 and at angles of incidence up to 10^{o}. The Reynolds number based on intake height was about 1.5×10^{6} for Mach numbers above 2 and 0.6×10^{6} for Mach numbers below 2. Some measurements at $M_{\infty} = 2.01$ were made at both Reynolds numbers.

The results confirm the findings of Part I of this Report that shock patterns can be used to predict accurately maximum mass flow and shock pressure recovery provided the assumption is made that the initial wedge angle is increased by just under one degree. The results also show that simple assumptions can be made as to the form of the shock pattern in order to extend these predictions into regions of shock detachment which arise inevitably when the intake is at large angles of incidence.

A simple correlation of losses other than shock losses with a 'turning loss' factor used in Part I, is found to serve equally well when the intake operates over a range of incidence from 0^{o} to 10^{o}.

---

* Replaces RAE Technical Report 71236 - ARC 33891

CONTENTS

1 INTRODUCTION

An extensive programme of wind tunnel tests has been carried out at RAE Bedford to investigate the internal performance of a particular rectangular intake both in a uniform flow field and on a fuselage. Ref.1 dealt with the performance in a uniform flow field at zero incidence and the purpose of the present Report is to extend this basic performance data to include the effect of incidence.

The data so far reported[1] were obtained in the 3ft × 4ft tunnel. Although the minimum Mach number of the tunnel is 2.5, by fitting a shock plate to the intake test rig as shown in Fig.1 a Mach number range of 1.7 to 2.5 was obtained and some advantage could be taken of the high stagnation pressure available in this tunnel. When using this shock plate the intake can be tested over a range of pitch angle by tilting the shock plate with respect to the intake. However because the maximum incidence of the tunnel pitch changing mechanism is limited to 20° tests on the isolated intake could only be done in this tunnel by restricting both the range of pitch angle and the range of intake free stream Mach number. The compromise adopted was to test the intake at Mach numbers of 2.01, 2.22 and 2.46 at angles of incidence of 0°, $2\frac{1}{2}^{\circ}$ and 5°.

Clearly tests involving the fuselage[2] at Mach numbers below 2.5 could not be done in the 3ft × 4ft tunnel and these had to be done in the 3ft × 3ft tunnel where supersonic Mach numbers up to 2 only can be obtained at stagnation pressures of about two-thirds of an atmosphere. To provide a datum for these tests and to provide a link between the data obtained from the two tunnels, the isolated intake has been tested in the 3ft × 3ft tunnel at Mach numbers of 1.70 and 2.01 through an incidence range of zero to 10°.

2 DESCRIPTION OF THE TEST RIG AND DETAILS OF THE MODEL

Fig.1 shows the intake and duct assembled on the General Intake Test Rig (GERTI) with shock plate attached, as used in the 3ft × 4ft supersonic wind tunnel at RAE Bedford. The arrangement used in the 3ft × 3ft tunnel is identical except that the shock plate and its supporting brackets are omitted. This rig has been described in detail in Ref.3. It consists of a sting support, a calibrated mass flow control and measuring unit, a system of hydraulic actuators for moving the compression surface ramps and an instrumented duct with interchangeable exit plugs for controlling and measuring the intake bleed flow.

The model is that used in Ref.1 where it is described in detail. The ratio of height to width at the entry plane is 1.54 and the geometry of the compression surface ramps, cowl and bleed are as shown in Fig.3. The first compression surface has a fixed angle δ_1 of 10°, and the shock from its leading edge theoretically falls on the cowl lip at a free stream Mach number of 2.43. The second compression surface is movable and is linked to the rear ramp so that a single hydraulic actuator moves both these surfaces inter-dependently. The gap between the second and rear ramps forms a slot for bleeding the boundary layer from the compression surfaces and this slot extends over the whole width of the intake. The geometry of the bleed exit and details of the interchangeable plugs which change the area of this exit and hence vary the bleed flow, are shown in Fig.4.

The area distribution through the intake and duct for various values of δ_2 is shown in Fig.5. The ratio of engine face cross-sectional area to maximum capture area is 0.88 and the distance from the cowl lip to the engine face is 9.89 times the intake height.

The nomenclature used throughout this Report is shown in Fig.6.

3 DETAILS OF THE TEST

3.1 Instrumentation

The standard mass flow control and measuring unit[3] is fitted with a cruciform rake having a total of 24 pitot tubes for measuring total pressure at the engine face station. The tubes are disposed for area-weighted averaging and the rake is rotatable to enable pressure surveys to be made in greater detail. Static pressure at the engine face is measured by using four holes equally spaced round the circumference. Additionally static pressure is measured in the venturi section of the mass flow measuring unit downstream of the engine face rake.

The bleed duct contains 12 pitot tubes for measuring total pressure and three holes for measuring static pressure arranged as shown in Fig.4.

Three rakes each containing six pitot tubes are used to measure the pressure distribution in the intake at the entrance to the fixed portion of the subsonic diffuser. The rakes are located in the cowl at the rear ramp hinge position. During all the tests done in the 3ft × 3ft tunnel although all three rakes were fitted measurements were made only on the centre rake.

All pressures were measured by means of self balancing capsule type manometers[4].

3.2 Test conditions

The tests were done partly in the 3ft × 4ft supersonic wind tunnel and partly in the 3ft × 3ft wind tunnel for reasons which have been explained in the Introduction.

Table 1 lists the free stream Mach numbers, angles of incidence and Reynolds numbers based on intake height, of the tests made in the two facilities.

Table 1

Tunnel	M_∞	α°	R_h
3 ft × 4 ft	2.46	0, $2\frac{1}{2}$, 5	1.28×10^6
	2.22	-5, 0, $2\frac{1}{2}$, 5	1.42×10^6
	2.01	0, $2\frac{1}{2}$, 5	1.50×10^6
	1.80	-5	1.53×10^6
3 ft × 3 ft	2.01	0, $2\frac{1}{2}$, 5, $7\frac{1}{2}$, 10	0.57×10^6
	1.70	0, $2\frac{1}{2}$, 5, $7\frac{1}{2}$, 10	0.69×10^6

3.3 Reduction of results

Pressure recovery and mass flow in both the engine and the bleed ducts were measured for a range of values of second ramp angle δ_2 for each Mach number and intake incidence, with a particular fixed bleed exit area. This series was then repeated for a number of different bleed exit areas including the case of zero bleed.

Pressure recovery is defined as

$$\frac{P_f}{P_\infty} \text{ or } \frac{P_B}{P_\infty} = \frac{1}{nP_\infty} \sum_1^n P_j$$

where P_∞ is the free stream total pressure

P_j is the pitot pressure at the jth tube in the rake at the engine face station in the case of P_f or in the rake in the bleed duct in the case of P_B

and n is the number of pressure points in the survey.

Mass flow ratio $\frac{A_\infty}{A_e}$ in both the engine and bleed ducts was calculated assuming the exit flows to be choked:-

$$\frac{A_\infty}{A_e} = \frac{P}{P_\infty} \frac{A_{ex}}{A_e} \left(\frac{A}{A^*}\right)_\infty$$

where A_e is the intake entry area

A_{ex} is the effective choked exit area as determined by calibration in the case of the engine duct. In the case of the bleed duct the exit area was not calibrated and A_{ex} was taken to be the geometric area of the bleed exit plug

$\frac{P}{P_\infty}$ is either the engine duct pressure recovery $\frac{P_f}{P_\infty}$ or the bleed duct pressure recovery $\frac{P_B}{P_\infty}$.

3.4 Accuracies

The major causes of uncertainty in the calculation of pressure recovery and mass flow are in the use of M_∞ and P_∞, particularly where, as in the case of the 3ft × 4ft tunnel tests, these are obtained from a calibration of the shock plate. It is believed that quantitatively the values of pressure recovery are subject to errors overall of about ±0.0025, while the values of mass flow are subject to errors of ±0.0025 at M_∞ = 1.70 and 2.01, increasing to ±0.006 at M_∞ of 2.46. The accuracy of setting of the second ramp angle is about 0.1 degree.

4 DISCUSSION OF RESULTS

The performance characteristics of the intake are shown in Figs.7 to 17, where engine face pressure recovery is plotted against total intake flow, i.e., engine duct plus bleed duct flows, and against bleed duct pressure recovery where appropriate. Because each characteristic is obtained at a constant value

of bleed exit area, as defined in Fig.4 by the exit plug number, the bleed mass flow at any point can be obtained from the bleed pressure recovery by reference to Fig.18. This shows the relationship between bleed pressure recovery and bleed mass flow for plugs number 4 and 8, at the Mach numbers used in the tests.

From these basic characteristics, variation of maximum total intake flow and engine face pressure recovery at critical flow conditions have been derived. As in Ref.1 the critical flow condition is defined as the point on the pressure recovery-mass flow characteristic where the total mass flow departs from the maximum value.

4.1 Maximum mass flow

4.1.1 General

Figs.19, 20 and 21 show the variation of maximum mass flow with second ramp angle δ_2 for Mach numbers of 2.46, 2.22, 2.01 and 1.70, and for various angles of incidence of the intake. For the Mach numbers 2.01 to 2.46 maximum mass flow is seen to be independent of bleed flow quantity provided this exceeds the value of 0.02. At a Mach number of 1.70 maximum mass flow is still dependent on bleed flow up to a bleed flow quantity of 0.05 when δ_2 is less than about three degrees. At larger values of δ_2 maximum mass flow becomes independent of bleed flow for bleed flow quantities in excess of 0.03.

4.1.2 Estimation of maximum mass flow from shock patterns

Fig.22 illustrates the general pattern of the variation of maximum mass flow, firstly, with angle of incidence when the free stream Mach number and intake compression geometry are kept constant, and secondly, with second ramp angle δ_2 when the free stream Mach number and angle of incidence are kept constant. Theoretical shock patterns appropriate to particular regions of the mass flow curve are also shown, together with the corresponding shock patterns which have been assumed for the purpose of estimating maximum mass flow. Following the evidence of Ref.1 which suggested that aerodynamically the initial wedge angle was effectively nearly 11° rather than 10°, an effective compression surface has been assumed as indicated in Fig.22, in which δ_1 is equal to 11°, the longitudinal position of the hinge nevertheless remains unchanged.

Throughout parts A and B of the mass flow curves the shock patterns are entirely regular, that is all shocks are attached, and shock pressure recovery and maximum mass flow have been calculated by the method of Ref.6, using the

effective compression geometry. For portion C of the curves the shock at the cowl lip theoretically is detached, but this has been ignored and the calculations carried out as for parts A and B. In the region D of the mass flow curve the second oblique shock theoretically is no longer attached at the hinge point. In this case the maximum mass flow has been calculated with the assumption that the flow velocity at the entry plane is sonic and that the pressure recovery downstream of the second oblique shock remains constant after shock detachment i.e., it remains at the pressure recovery associated with point 'c' on the curves. In region E, that is where the angle of incidence of the intake is sufficiently large, the leading-edge shock is theoretically detached. In this condition the assumption has again been made of sonic velocity at the entry plane but now the pressure recovery is assumed to be that associated with point 'd' on the mass flow curve, which is the point where the leading-edge shock just detaches.

Estimates of maximum mass flow derived in the above manner are shown throughout Figs.19, 20 and 21 by chain-dotted curves.

4.1.3 The effect of internal contraction on the estimates of maximum mass flow

Estimates made in the manner of section 4.1.2 are only valid when the maximum flow entering the intake is largely determined by the external oblique shock system with the terminal shock situated at the cowl lip; there being minor deviations only caused for example by the detachment of the shock at the cowl lip due to slightly too large a turning angle being demanded at this point. However if the duct downstream of the entry plane is contracted so that the flow behind the normal shock is reaccelerated to sonic velocity then the maximum flow will be controlled by this 'second throat' and will proportionately decrease as this throat decreases in area.

For a given value of M_∞ and assuming an effective compression surface geometry in which δ_1 equals 11°, δ_2 defines the Mach number approaching the cowl lip (M_2 in Fig.6). From this Mach number the onedimensional area ratio required to start the duct flow can be calculated i.e., the area ratio A_t/A_i required to accelerate the subsonic flow behind a normal shock occurring at $M = M_2$ to sonic velocity. This area ratio is shown in Figs.23a and 23b, plotted against δ_2 for each Mach number and for the angles of incidence used in the tests. Superimposed on these curves is curve A which is the geometric contraction ratio A_t/A_i for the duct of this particular intake.

Comparison of these curves indicates that with zero bleed the duct is over-contracted throughout most of the test range and choking will therefore take place at the intake throat A_t. The effect of this choking on the maximum mass flow estimated in accordance with section 4.1.2 can be calculated readily and is shown throughout Figs.19, 20 and 21 by the dotted curves.

4.1.4 Comparison of measured and estimated maximum mass flows at zero bleed

The good agreement between the mass flows measured at zero bleed and the predicted values, which in Ref.1 was found to exist at zero incidence, is confirmed throughout the entire incidence range. However it is again obvious, as it was in Ref.1 that this agreement does not extend to values of δ_2 below about 5^o. This is probably due to the duct having an effective contraction ratio differing from that measured geometrically; the difference being most exaggerated at low values of δ_2 as suggested by curve B of Fig.23. When δ_2 has values below 5^o the minimum duct area is at the rear hinge well downstream of the entry plane and large viscous effects might be expected. This, together with the possibility of some separation on the rear ramp and a contraction ratio which is already high, probably accounts for the significant reduction in effective throat area. When δ_2 has values above 5^o the throat moves upstream to the leading edge of the rear ramp and with a more favourable contraction ratio the viscous effects no longer influence the choking area to the same extent. The ratio between the effective minimum area and the effective inlet area is then not significantly different to the ratio of their geometric values, that is, curves A and B of Figs.23a and 23b become more or less coincident.

4.1.5 The effect of bleed on maximum mass flow

In the absence of subsonic forespill changes in the maximum mass flow will only be brought about by modification of the external shock pattern. For this particular intake in all such cases the measured maximum mass flow is independent of bleed flow quantity and is always in fairly close agreement with the mass flow predicted by using an effective compression surface geometry in which δ_1 is equal to 11 degrees. It appears therefore that bleed, applied in the location used in this intake, has little or no effect on the mechanism by which this effective compression surface geometry is produced.

The duct minimum area is always downstream of the entry plane and as Figs.23a and 23b show, throughout much of the test regime, the intake, without bleed is operating in an unstarted mode. However with the application of bleed the intake can be made to operate in a started mode, the amount of bleed flow required depending upon free stream Mach number, δ_2 and angle of incidence. Perhaps the immediate effect of bleed flow is on the effective throat. By restoring the minimum duct area to its geometric value the internal contraction of the intake would be approximately that given by curve C of Figs.23a and 23b. Moreover because the bleed suction is upstream of the minimum duct area, this bleed flow, while increasing the total mass flow causes no loss in engine duct mass flow until the intake is choked at the entry plane. Thus the intake operates in a started mode for all values of δ_2 above about 3^o, provided bleed flow quantity is above 0.02 at Mach numbers of 2.01, 2.22 and 2.46 and is above 0.03 at M_∞ of 1.70. The spillage which occurs at the higher values of δ_2 in each case being due mainly to shock detachment at the cowl lip caused by excessive flow turning at the cowl inner or outer surface.

Because of the excessive internal contraction of the duct, few measurements have been made at values of δ_2 less than three degrees. However the evidence of $M_\infty = 1.70$, $\delta_2 0^o$ does suggest that in this region, probably because of the location of the throat, the bleed is much less effective in bringing about an increase in effective minimum area.

4.2 Pressure recovery

Fig.24 shows the pressure recovery at critical flow conditions plotted against δ_2 for the Mach numbers 2.46 and 2.22 at constant bleed flows of $(A_\infty/A_e)_B$ equal to 0, 0.03 and 0.06. Shock recoveries calculated for a leading wedge angle of 11^o are included for comparison.

At zero bleed flow the losses other than shock losses can be calculated by the method of Ref.5 and these estimates too have been included in Fig.24. There is a considerable difference between these estimates and the pressure recoveries measured at zero bleed flow at all angles of incidence. This difference has been correlated to a factor compounded from the theoretical normal shock Mach number and the angle of turning between the second ramp and the rear ramp. This correlation is shown in Fig.29.

At these free stream Mach numbers there is a substantial improvement in pressure recovery with increasing bleed flow. For bleed flow quantities up to

$(A_\infty/A_e)_B = 0.06$, the rate of increase of pressure recovery with bleed flow, $d(P_f/P_\infty)/d(A_\infty/A_e)_B$ has a value of just under 2; apparently independent of Mach number, δ_2 or angle of incidence. The measurements suggest that with the cowl lip shock attached the variation of pressure recovery with δ_2 follows the theoretical shock recovery curve and if allowance is made for skin friction losses in the duct, the theoretical recovery can be achieved with a bleed flow $(A_\infty/A_e)_B$ of about 0.06. The values of δ_2 used in the tests at incidence were deliberately chosen to be in the region of shock detachment at the cowl lip due to excessive flow turning. The results indicate that the onset of cowl lip shock detachment produces a significant loss in pressure recovery. This is particularly so at $M_\infty = 2.46$ where the first oblique shock is close to the cowl lip.

The total pressure distributions at three stations across the duct at the rear hinge position for Mach numbers of 2.46 and 2.22 with bleed exit plugs 0, 4, and 8 are shown in Figs.27 and 28. The large low pressure region adjacent to the rear ramp, which was a feature at zero incidence is no longer quite so obvious at intake incidences of 2.5 and 5 degrees. However there is now evidence of a low pressure region in the middle of the flow at the station midway between the centre line and the endwall, which is almost completely eliminated by increasing bleed. High peak values of recovery, more consistent with calculations of shock recovery based on two oblique shocks only, occur in the middle of the flow near the duct endwalls at all angles of incidence, suggesting that in this region the terminal shock compression is through a fan of oblique shocks, giving effectively isentropic compression.

For the lower Mach numbers $M_\infty = 2.01$ and 1.70, critical point pressure recovery as a function of δ_2 is shown in Figs.25 and 26, together with predicted shock recoveries. At $M_\infty = 2.01$ there is a similar substantial improvement in pressure recovery with increasing bleed to that which occurred at the higher Mach numbers: but this now applies only up to a bleed flow quantity of 0.03. Beyond this point the rate of increase of pressure recovery with bleed flow falls off quite sharply. However this is probably simply a reflection of the change in external shock pattern. Constant maximum total mass flow is achieved when $(A_\infty/A_e)_B$ reaches about 0.03; the external shock pattern remaining unchanged as bleed flow increases further. In this condition the variation of pressure recovery with δ_2 follows closely the shape of the curves of predicted shock recovery. When allowance has been made for skin

friction losses, the theoretical pressure recovery is almost achieved and further increase of bleed flow inevitably achieves very little increase in engine face recovery. After the detachment of the second oblique shock, the maximum pressure recovery tends to the value of two shock recovery i.e., one oblique shock plus a normal shock.

At M_∞ = 1.70 there is only a small improvement in pressure recovery with bleed, and even then only for bleed flows up to 0.03. Bleed flow quantities in excess of this amount have no further effect on pressure recovery. This again is a reflection of the change in external shock pattern; constant maximum total mass flow being achieved with this amount of bleed when δ_2 has values above about 3°. In this condition, i.e. where the external shock pattern has become fixed and where the two oblique shocks are attached, the measured pressure recovery although following the shape of the curves of predicted shock recovery, falls well short of the theoretical value by about six per cent. Where the second oblique shock detaches, even with bleed, the maximum pressure recovery falls about five per cent short of the value of two shock recovery. At high angles of incidence, where the leading-edge shock detaches the pressure recovery tends very quickly to the normal shock value.

At the lower Mach numbers, M_∞ = 2.01 and 1.70, the difference between measured and estimated recovery at zero bleed, after allowing for extra-to-shock losses based on Ref.5 is quantitatively less than for the higher Mach numbers. However the additional or 'turning' losses for these Mach numbers provide the least well correlated points on Fig.29.

4.3 Pressure recovery and mass flow at negative incidence

As part of a separate investigation involving this intake a few characteristics were obtained with the intake at an angle of incidence of -5°, at free stream Mach numbers of 1.80 and 2.22 with bleed exit plug number 4 fitted. The characteristics are not themselves included in this Report, but both maximum mass flow and critical point pressure recovery have been derived and are shown plotted against δ_2 in Fig.30. Theoretical curves calculated from the intake shock patterns are also included. There is again good agreement between calculated and measured mass flows and the extra-to-shock losses are shown to be of the same order as in the case of positive incidence.

4.4 Stable flow range and flow distortion at the engine face

Stable flow range is defined as the fraction by which the maximum mass flow can be reduced before the onset of buzz. Buzz in this case is 'big buzz' as seen using the schlieren optical system and is therefore not a very precise measurement.

The variation of stable flow range with δ_2 for zero bleed and when bleed exit plug 4 was used is shown in Fig.31 for Mach numbers of 2.46 and 2.22; and in Fig.32 for Mach numbers of 2.01 and 1.70. Based on the Ferri criterion of the vortex sheet impinging on the cowl lip causing the onset of instability, predictions of stable flow ranges have been made using the method given in Ref.6, and these have been included in the figures.

At Mach numbers of 2.01 and 1.70, at certain angles of incidence the second oblique shock detaches and for this condition, as also for the condition when $\delta_2 = 0^\circ$, a two shock system only exists, i.e., the first oblique shock followed by the detached shock, downstream of which the flow is subsonic. Use of this shock pattern in the method of Ref.6 leads to the discontinuities apparent in the predicted curves given in Fig.32.

Where the second oblique shock is attached the method appears to predict the stable flow range with fair success, but where the two shock system exists the method is less successful. In particular the step predicted at second oblique shock detachment is not reflected in the measurements, which indicate a progressive increase in stable flow range with δ_2 beyond this detachment point. When the first oblique shock detaches the stable flow range appears to reach a constant maximum value of about 50 per cent.

During each intake characteristic one or two comprehensive pressure surveys were made at the engine face. The flow distortion parameter DC_{60} has been derived from these surveys and is shown in Fig.33 for Mach numbers of 2.46 and 2.22, and in Fig.34 for Mach numbers of 2.01 and 1.70. In general the distortion level remains fairly constant and of the order of -0.02; variation of angle of incidence having no significant effect. There is some slight evidence that large bleed flows $[(A_\infty/A_e)_B > 0.04]$ have a detrimental effect, due probably to the adverse pressure gradient imposed on the flow on the wall opposite to the region where the bleed flow is being removed, which might produce thickening or separation of the boundary layer on the cowl undersurface.

4.5 The effect of Reynolds number

At a Mach number of 2.01 a number of identical characteristics were done in both the 3ft × 4ft tunnel at a Reynolds number based on intake entry height of 1.50×10^6 and in the 3ft × 3ft tunnel at a Reynolds number of 0.57×10^6. These characteristics are shown together in Figs.35, 36 and 37 for angles of incidence of 0°, $2\frac{1}{2}^\circ$ and 5°. In Fig.38 the characteristics obtained at $M_\infty = 1.70$, $\alpha 0^\circ$ at a Reynolds number of 0.69×10^6 are compared with the characteristics obtained at the same Mach number and angle of incidence but at a Reynolds number of 1.54×10^6.

At $M_\infty = 2.01$ when the intake is operating supercritically, whether in the started or unstarted mode, there is little significant difference between the maximum mass flows and the critical point pressure recoveries at the two values of Reynolds number. In the subcritical condition there are some significant differences in pressure recovery. In general increasing Reynolds number enhances pressure recovery, but at zero intake incidence, without bleed the opposite appears to be the case.

At $M_\infty = 1.70$ where the intake is always in the unstarted mode, the lower Reynolds number leads to a reduction in both maximum mass flow and pressure recovery.

No marked changes in distortion level with Reynolds number were detected.

5 CONCLUSIONS

Measurements have been made of the internal performance of a rectangular intake having a variable second-wedge angle. The measurements have been made at Mach numbers of 2.22 and 2.46 through a range of angles of incidence of the intake of zero to 5 degrees; and at Mach numbers of 1.70 and 2.01 through a range of incidence of zero to 10 degrees.

The Reynolds number based on intake entry height for the Mach numbers 2.22 and 2.46 were respectively 1.42 and 1.28×10^6, while those for the Mach numbers 1.70 and 2.01 were respectively 0.69 and 0.57×10^6. Additionally some measurements were made at Mach numbers of 1.70 and 2.01 at Reynolds numbers of 1.54 and 1.50×10^6 respectively.

The results confirm the findings of Ref.1 that shock patterns can be used to predict maximum mass flow and pressure recovery and indicate that simple assumptions can be made to extend these predictions into regions of shock detachment which are inevitable when the intake is at large angles of incidence.

The effective compression geometry may be different from the real geometry with an apparent increase in initial compression angle of as much as one degree. The exact nature of this effect is not clear and could well be investigated.

In using the method of Ref.5 to estimate losses other than shock losses some refinement is needed to take account of flow turning within the intake, particularly at high values of second ramp angle.

Throughout the range of incidence in which the tests were done, no marked changes in distortion level were detected.

NOTATION

(See also Fig.6)

A	cross-sectional area
CL	cowl lip shock detached
DC_{60}	Distortion parameter = $\dfrac{(P_f)_{minimum} - (P_f)_{mean}}{(\frac{1}{2}\rho V^2)_f}$ taken over the worst 60^o sector
FO	first oblique shock detached
M	Mach number
P	total pressure
p	static pressure
R_h	Reynolds number based on intake entry height
SFR	stable flow range
SO	second oblique shock detached
V	velocity
w	width of intake
X	distance downstream of cowl lip
z	lateral distance from duct sidewall
α	angle of incidence of intake relative to free stream with intake leading edge horizontal
δ_1	angle between first compression surface and free stream ahead of intake
δ_2	angle between first and second compression surfaces
ω	angle between front and rear movable ramps

Subscripts

c	at critical flow conditions
B	in the bleed
e	in the intake entry plane
ex	in the duct exit plane
f	at the engine face
i	at the cowl lip
r	at the rear hinge position
t	at the section of minimum duct area
T	total i.e., engine plus bleed
X	at station X
∞	in the free stream ahead of the intake
1	in the region behind the first oblique shock
2	in the region behind the second oblique shock

REFERENCES

No.	Author	Title, etc.
1	C. S. Brown E. L. Goldsmith	Measurement of the internal performance of a rectangular air intake with variable geometry. Part I. RAE Technical Report 71159 (ARC 33681) (1971)
2	C. S. Brown E. L. Goldsmith	Measurement of the internal performance of a rectangular air intake having variable geometry. Part IV. Intake mounted on a fuselage. RAE Technical Report 72136 (1972)
3	E. L. Goldsmith	Variable geometry intakes at supersonic speeds. Some techniques and some test results. Agard Conference Proceedings No.34 (1968)
4	G. F. Midwood R. W. Hayward	An automatic self-balancing capsule manometer. ARC CP 231 (1955)
5	J. Seddon	Boundary layer interaction effects in intakes with particular reference to those designed for dual subsonic and supersonic performance. ARC R & M 3565 (1966)
6	I. McGregor	Some theoretical parameters relevant to the performance of rectangular air intakes with double-ramp compression surfaces at supersonic speeds. RAE Technical Report 71232 (ARC 33616) (1971)

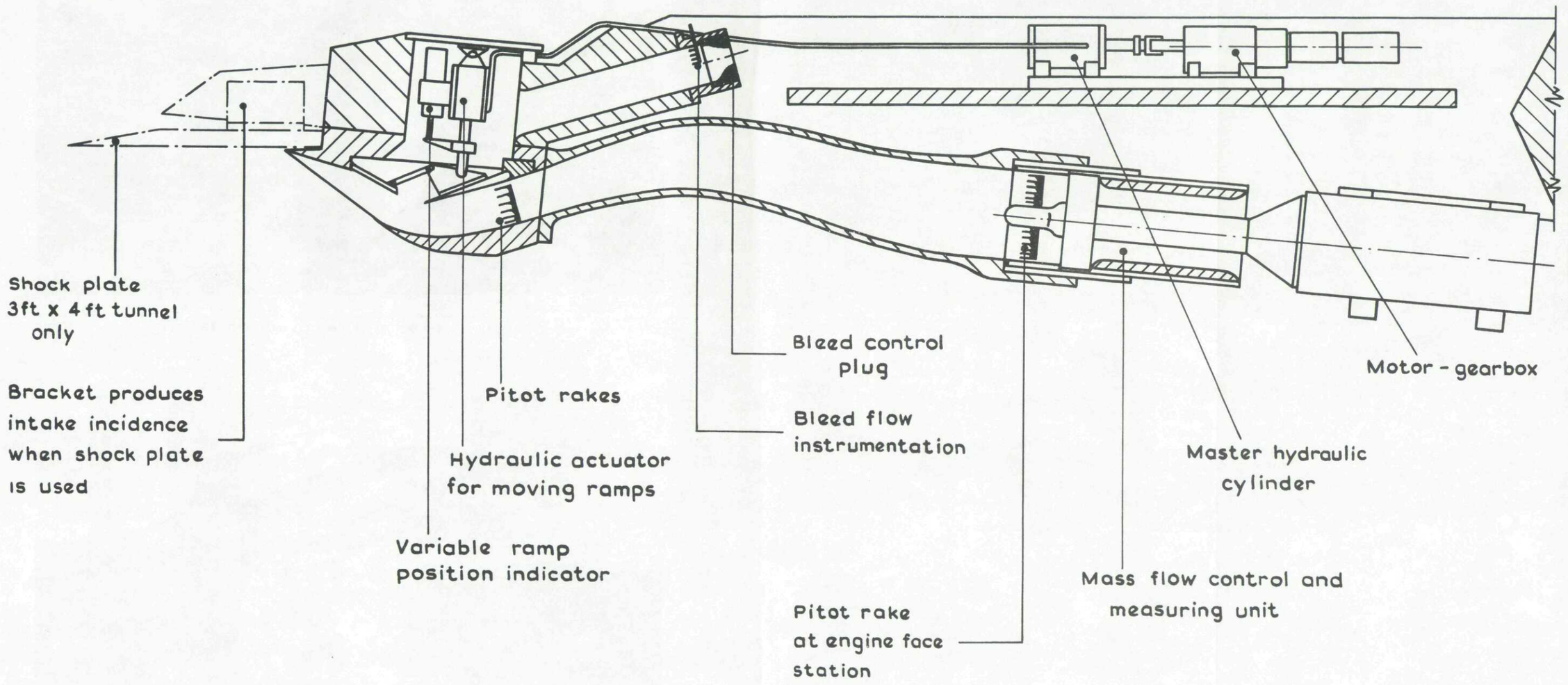

Fig.1 Arrangement of variable geometry rectangular intake on intake test rig

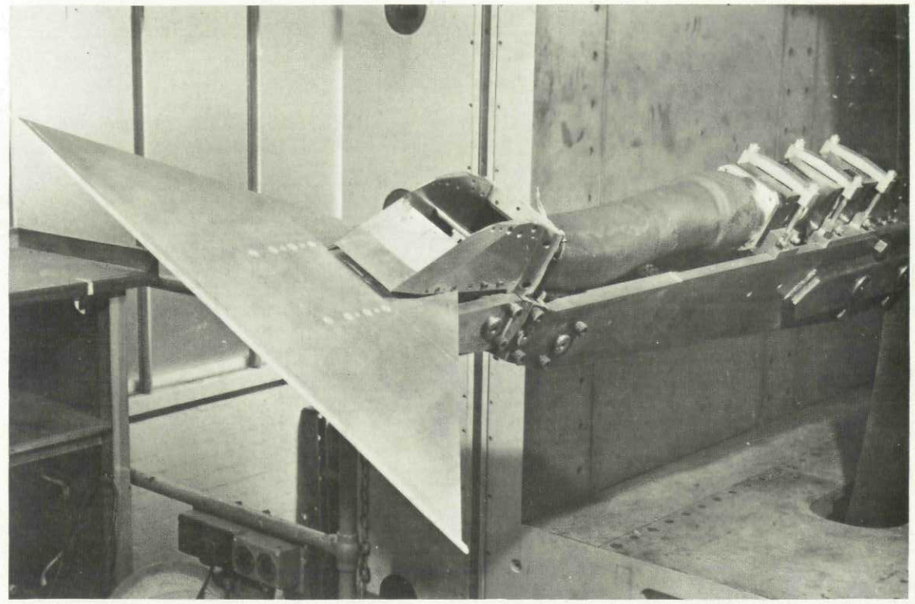

Fig.2(a). Intake (cowl removed) on test rig

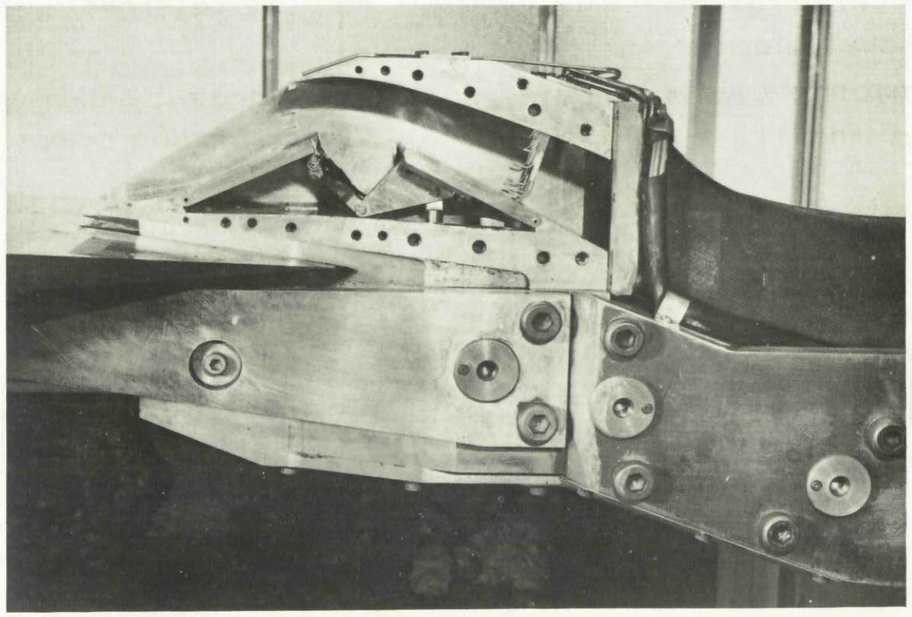

Fig.2(b). Intake with one endwall removed

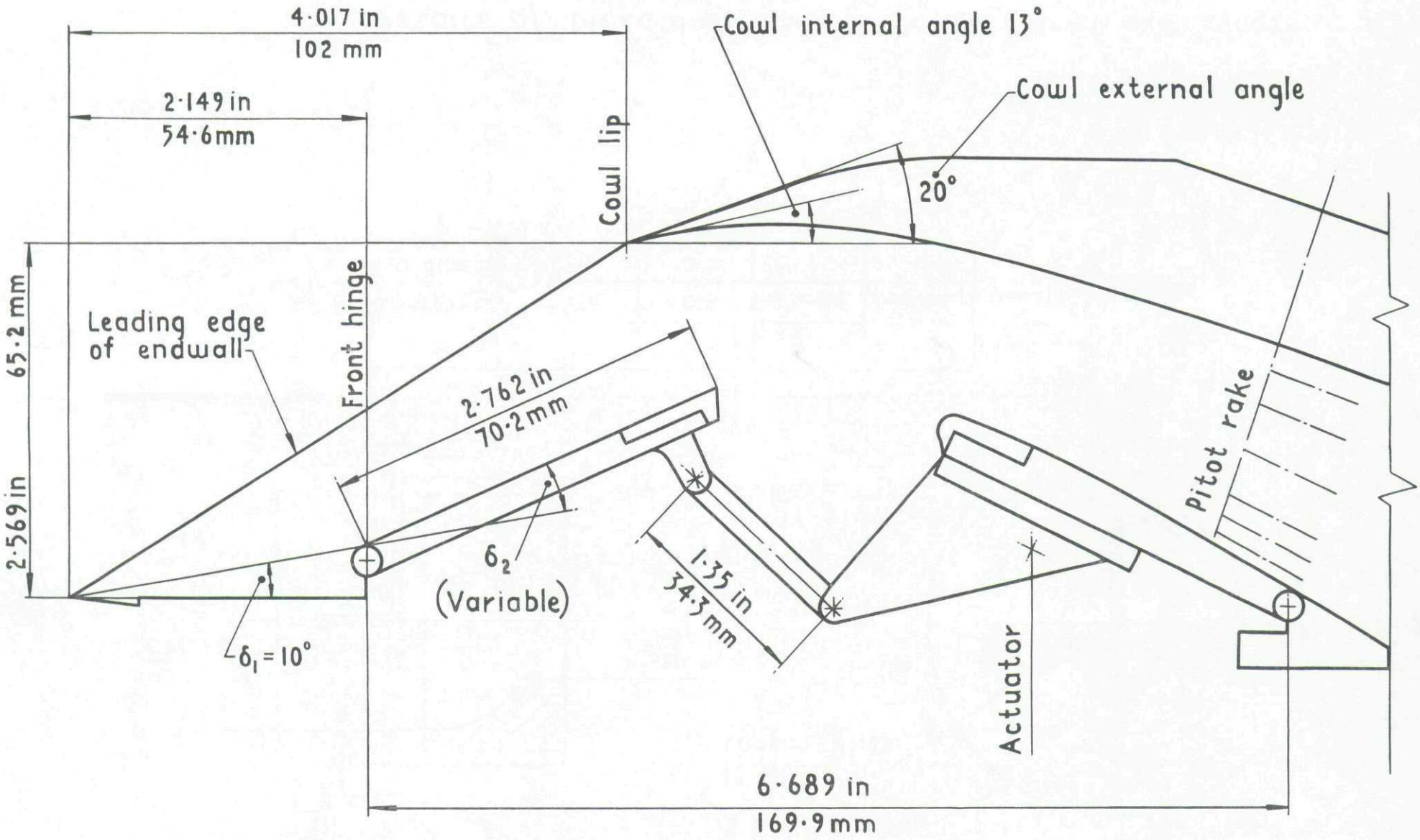

Fig. 3 Geometry of compression surface ramps, cowl and bleed

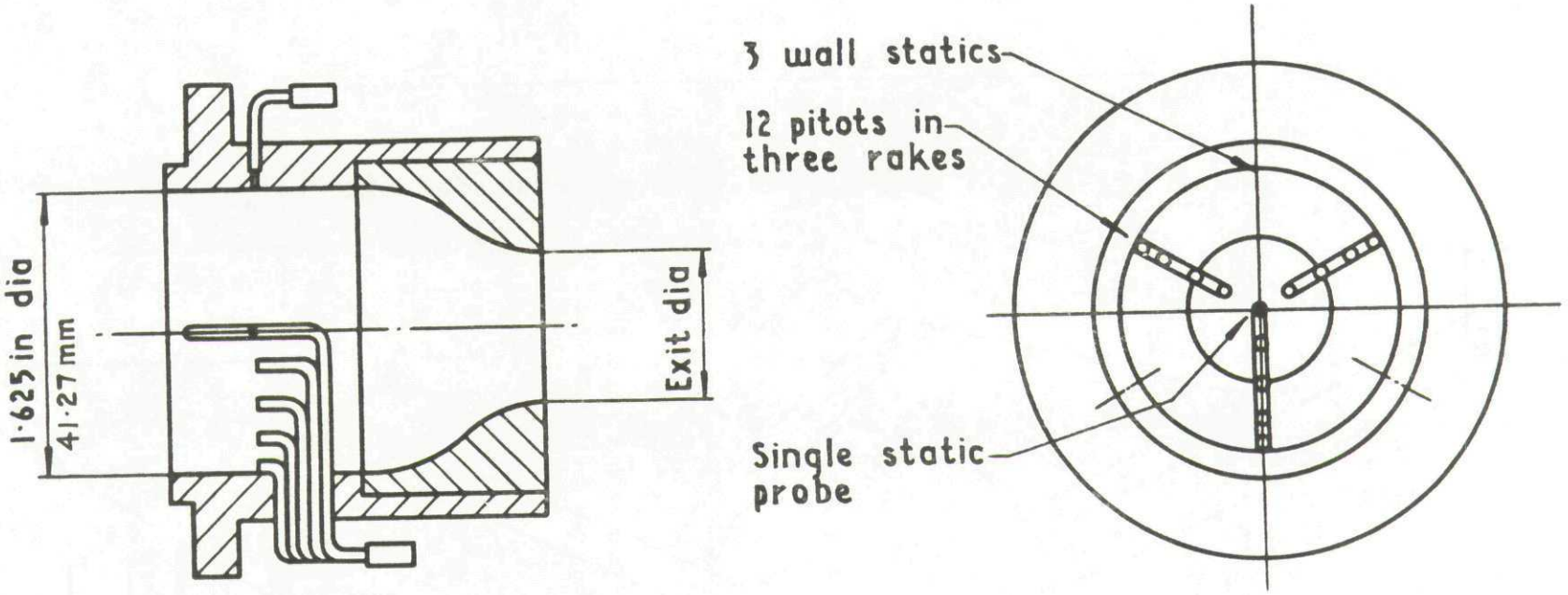

Plug No		0	4	8
Exit diameter	in	0	0·803	1·1435
	mm	0	20·40	29·04

Fig.4 Details of bleed instrumentation and bleed exit plugs

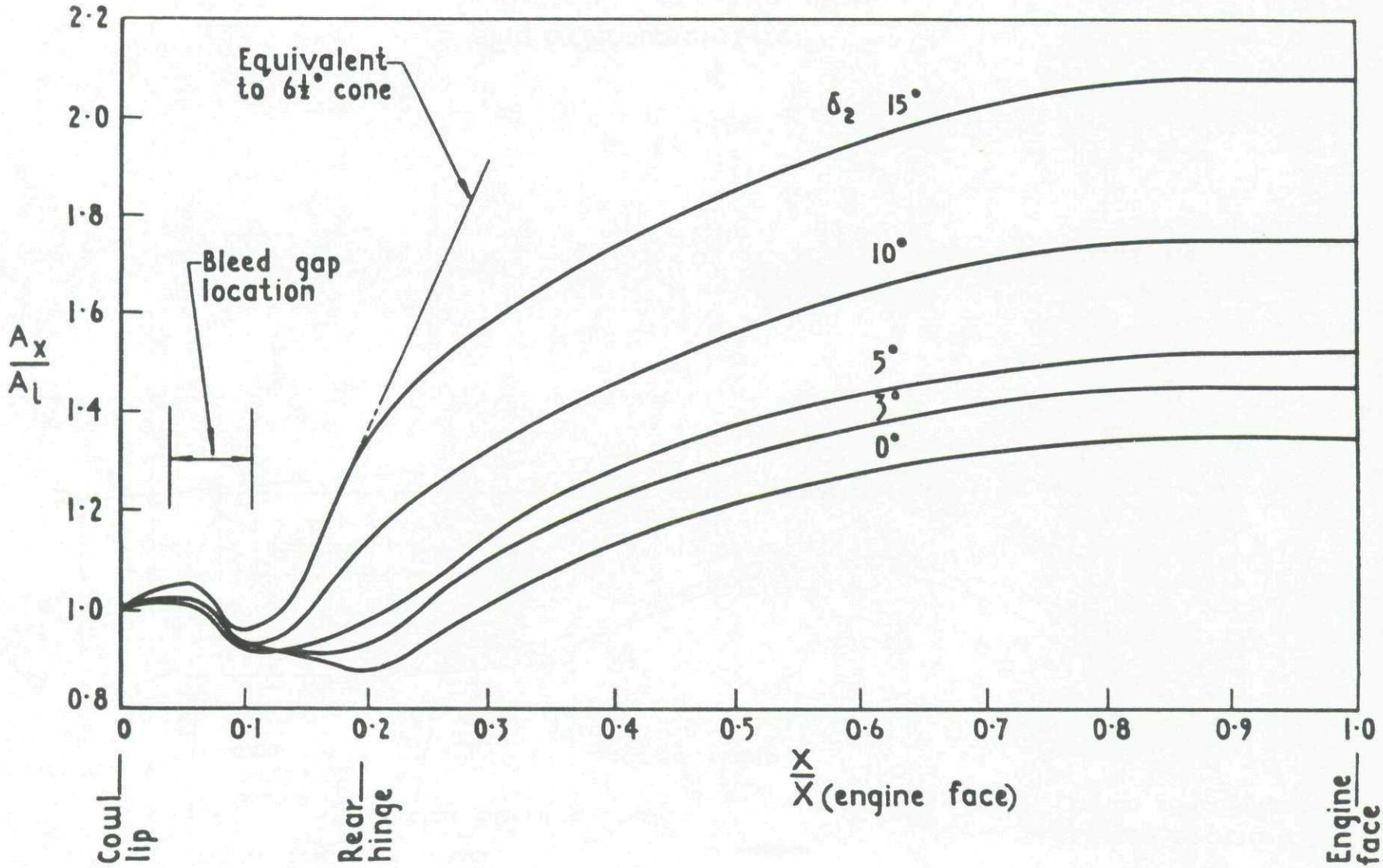

Fig.5 Area distribution through intake and duct

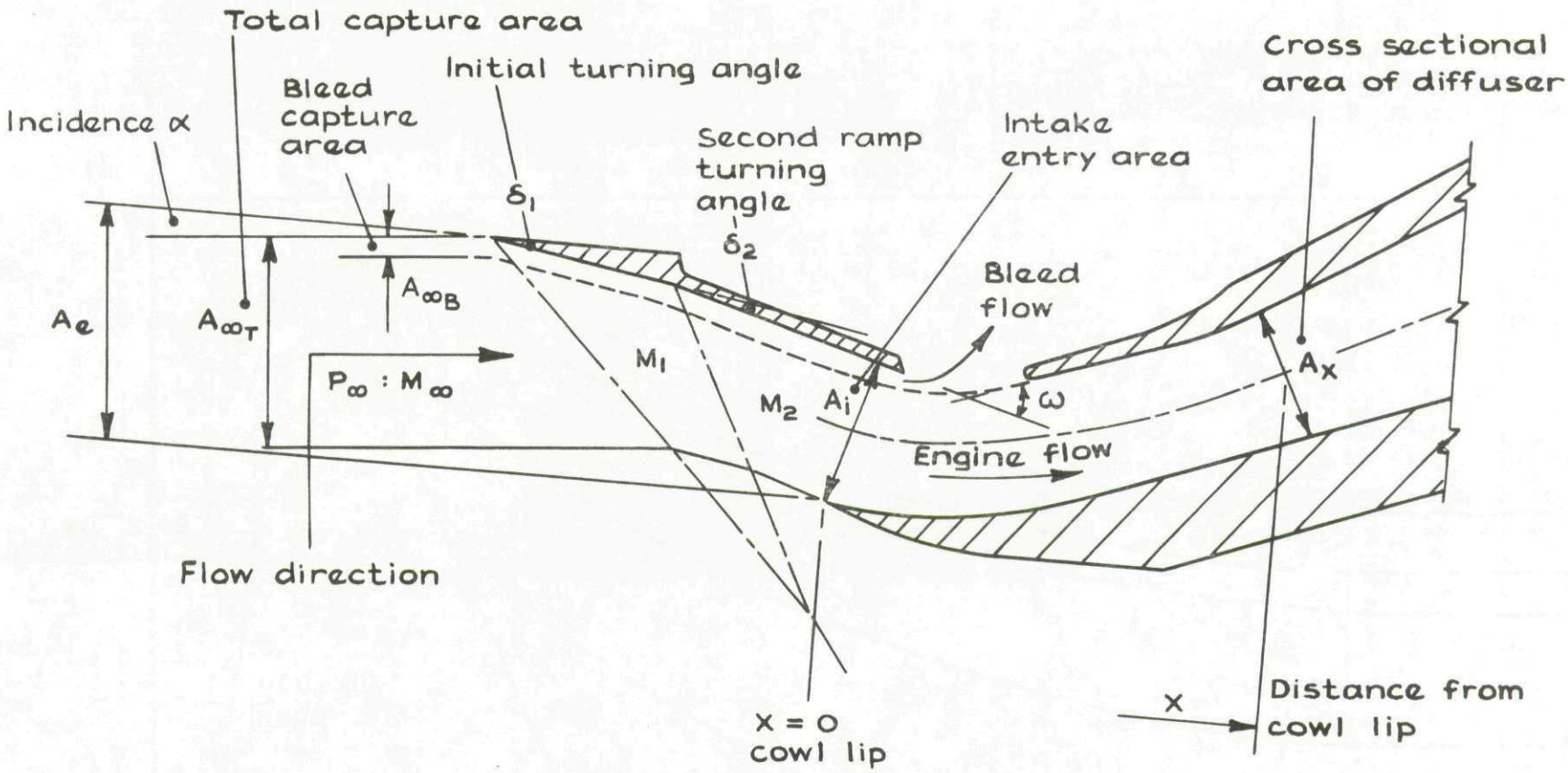

Fig.6 Nomenclature

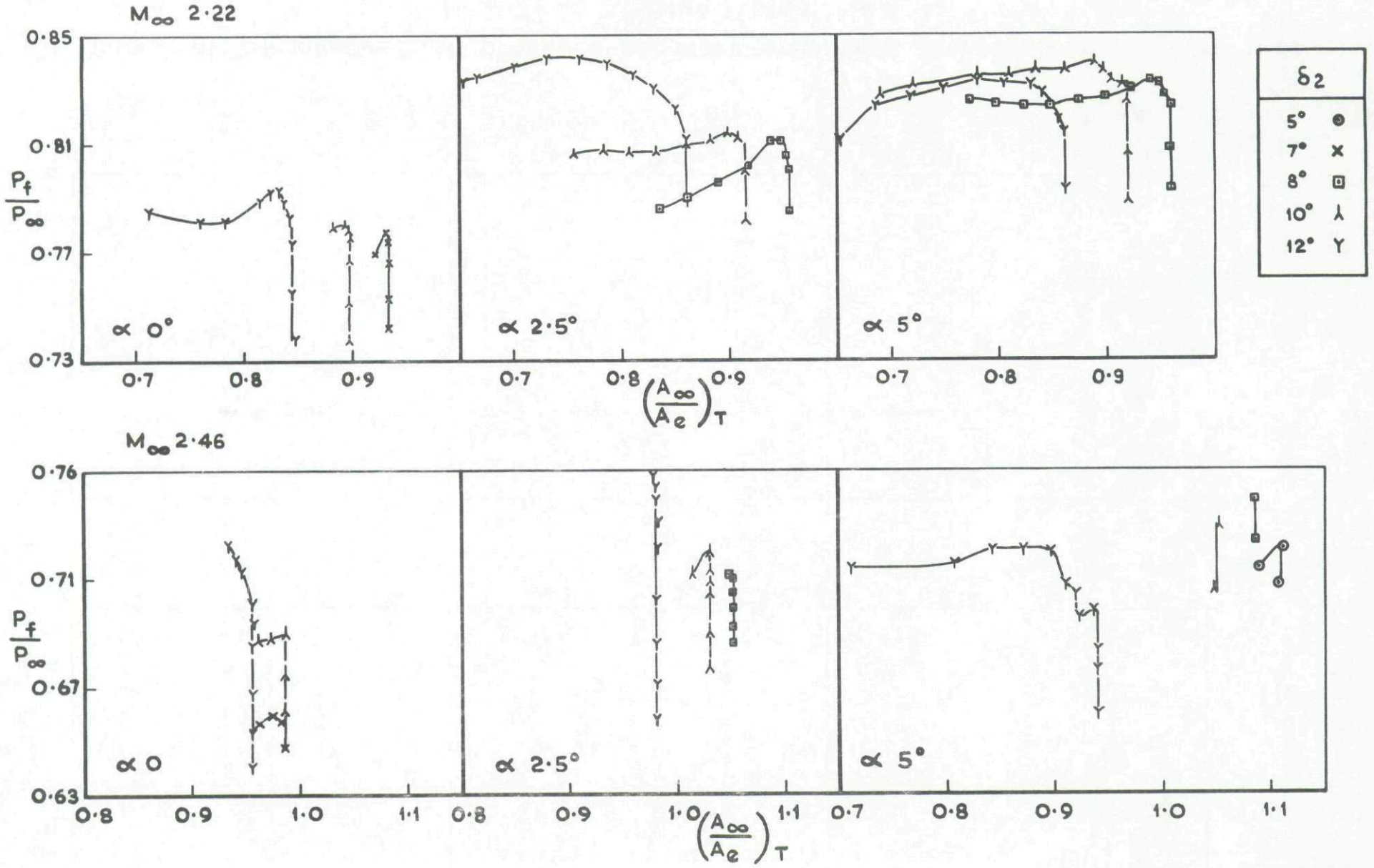

Fig.7 Variation of engine face pressure recovery with mass flow. Zero bleed
M_∞ 2·22 & 2·46

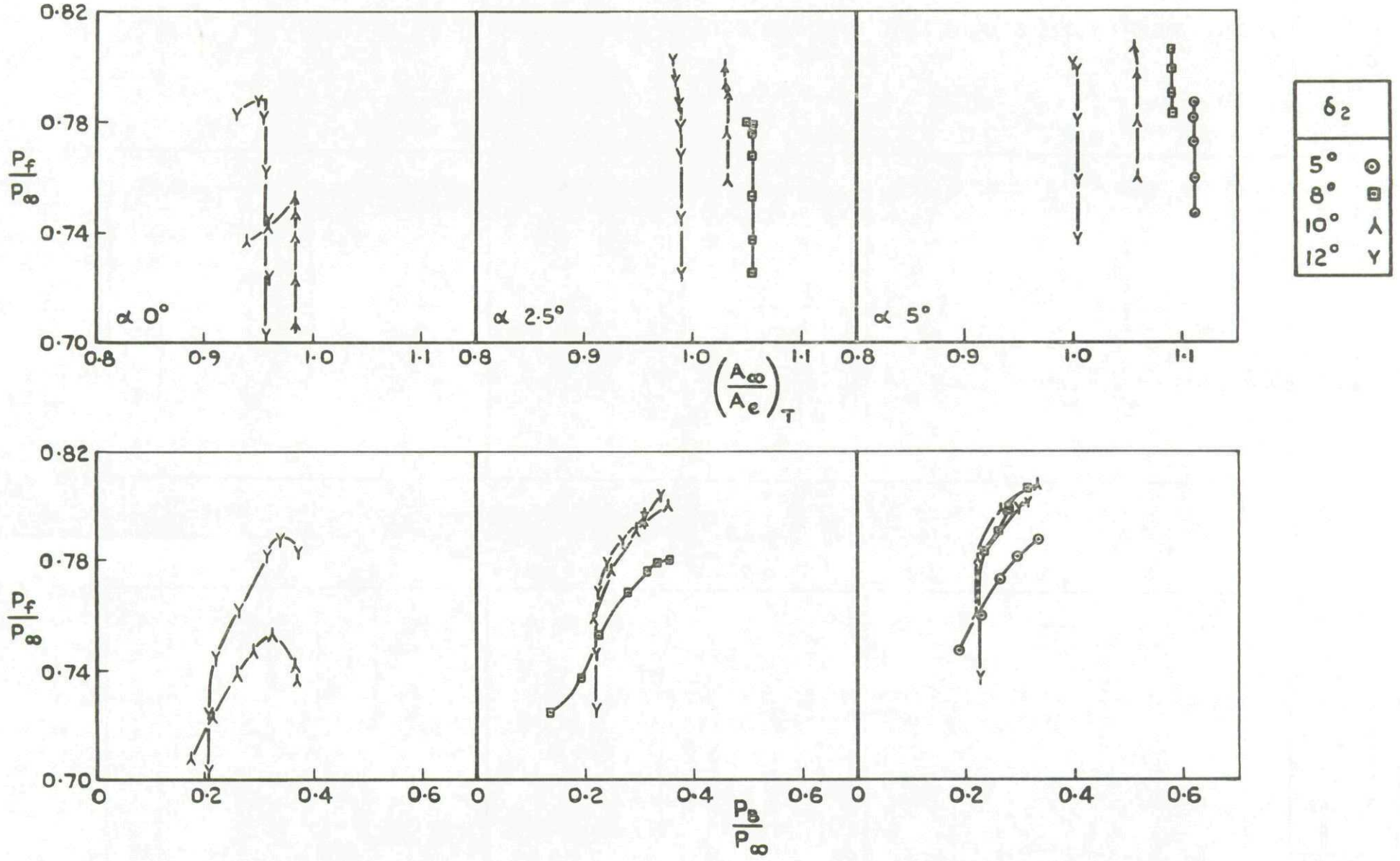

Fig. 8 Variation of engine face pressure recovery with mass flow & bleed pressure recovery

M_∞ 2·46 Bleed plug No 4

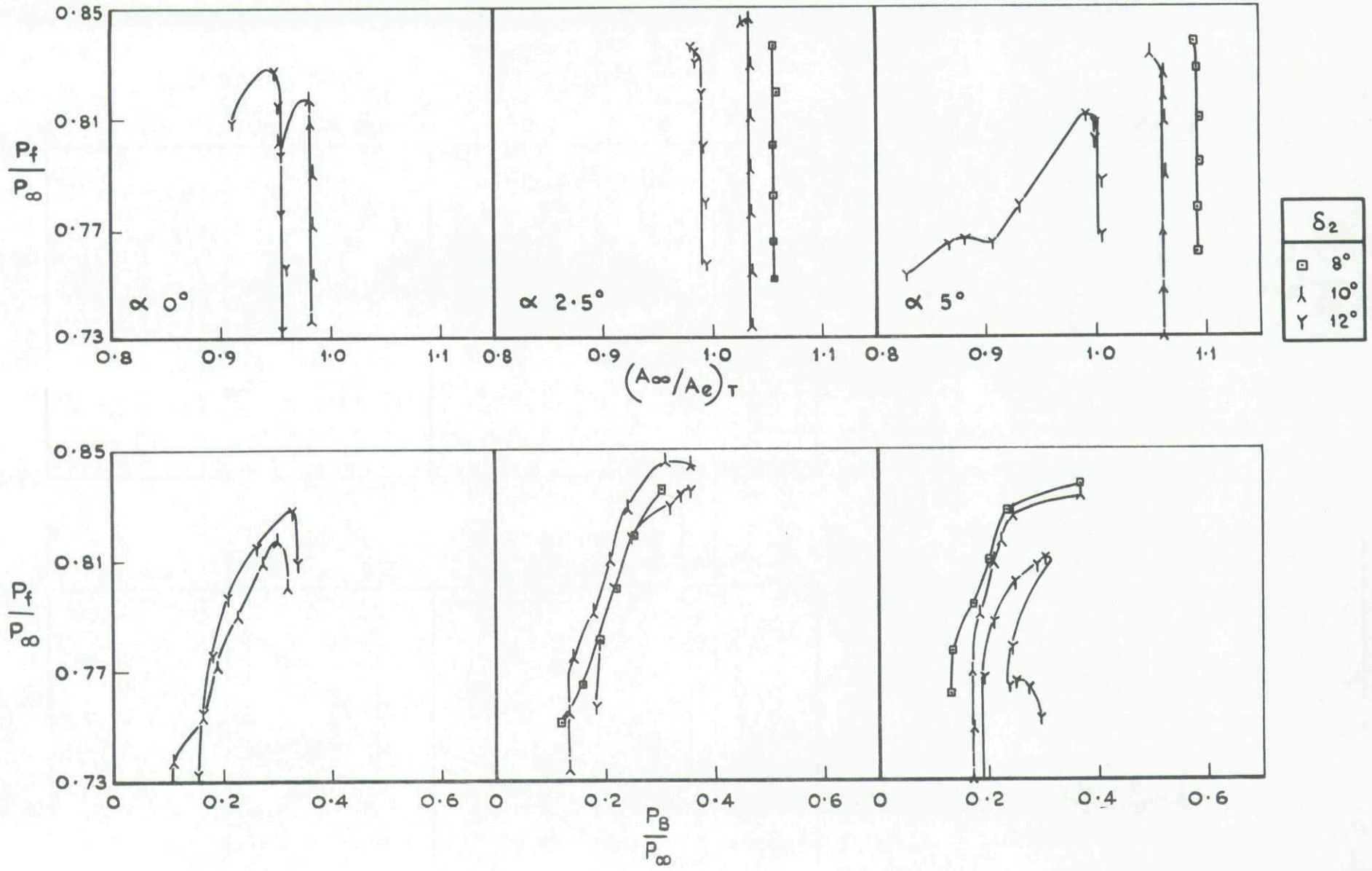

Fig.9 Variation of engine face pressure recovery with mass flow & bleed press: recovery
M∞ 2·46 Bleed plug No 8

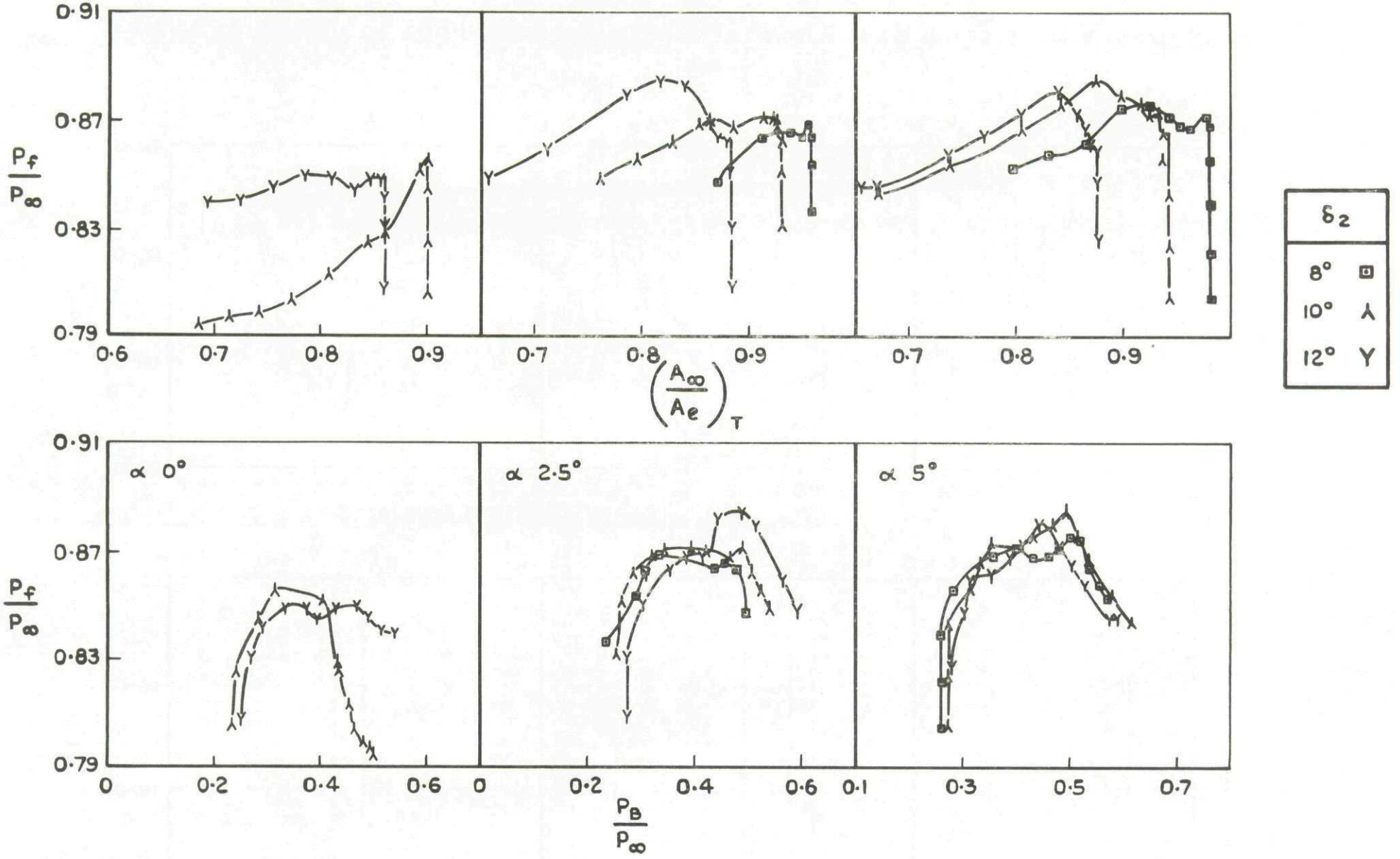

Fig.10 Variation of engine face pressure recovery with total mass flow & bleed pressure recovery. M_∞ 2·22. Bleed plug No 4

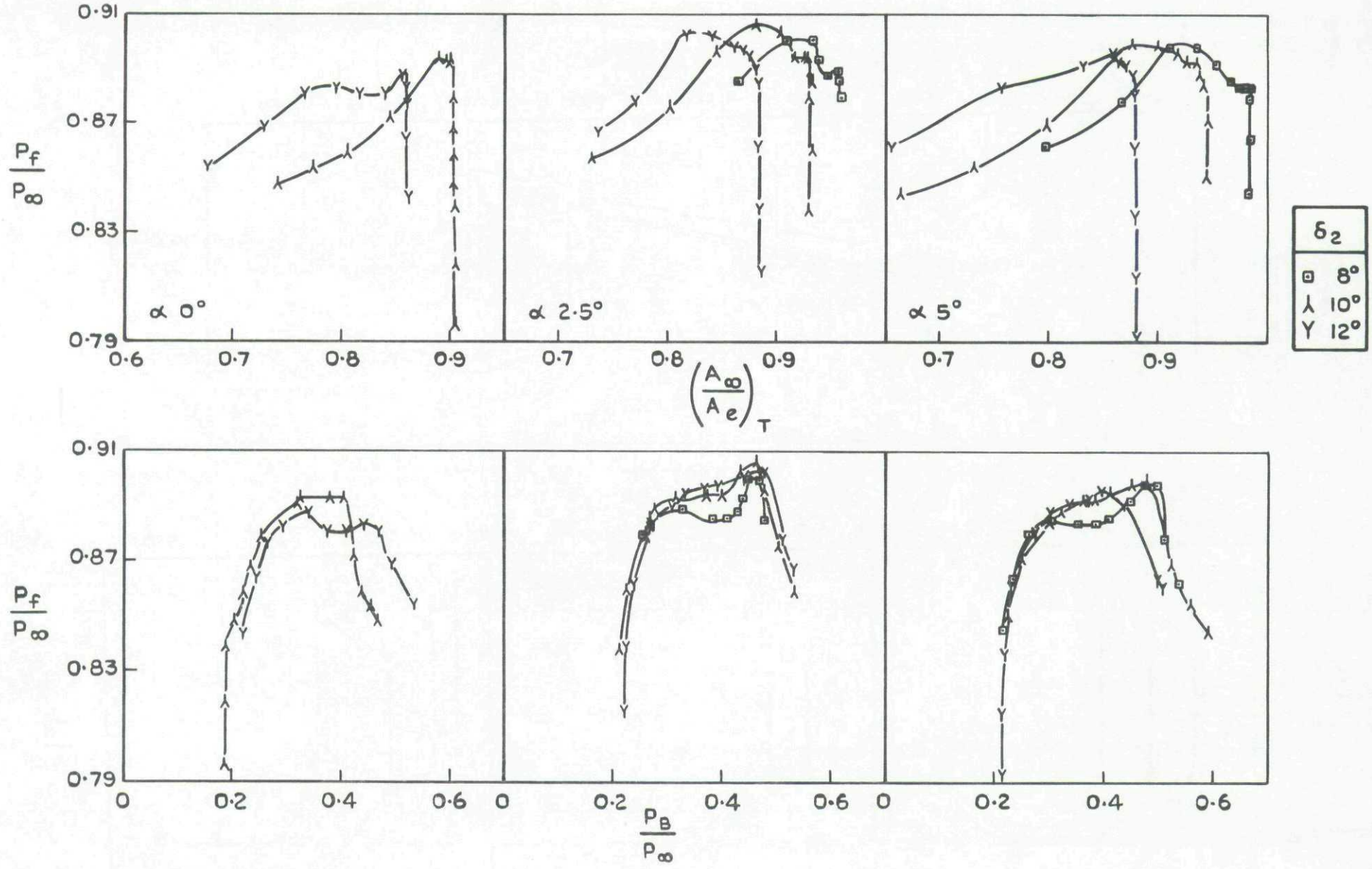

Fig.11 Variation of engine face pressure recovery with total mass flow & bleed pressure recovery. M_∞ 2·22. Bleed plug No 8

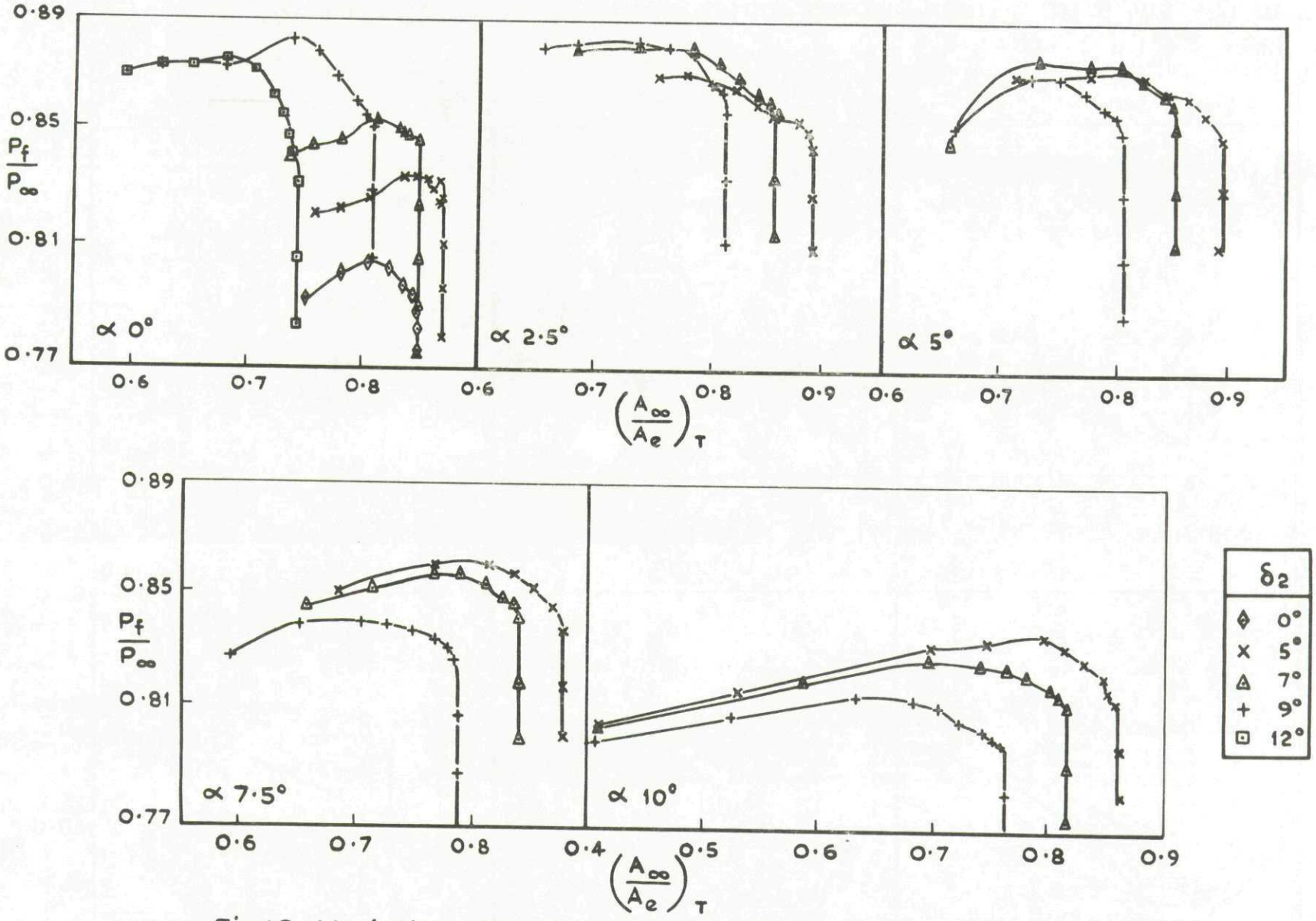

Fig.12 Variation of engine face pressure recovery with total mass flow. M_∞ 2·01. Zero bleed

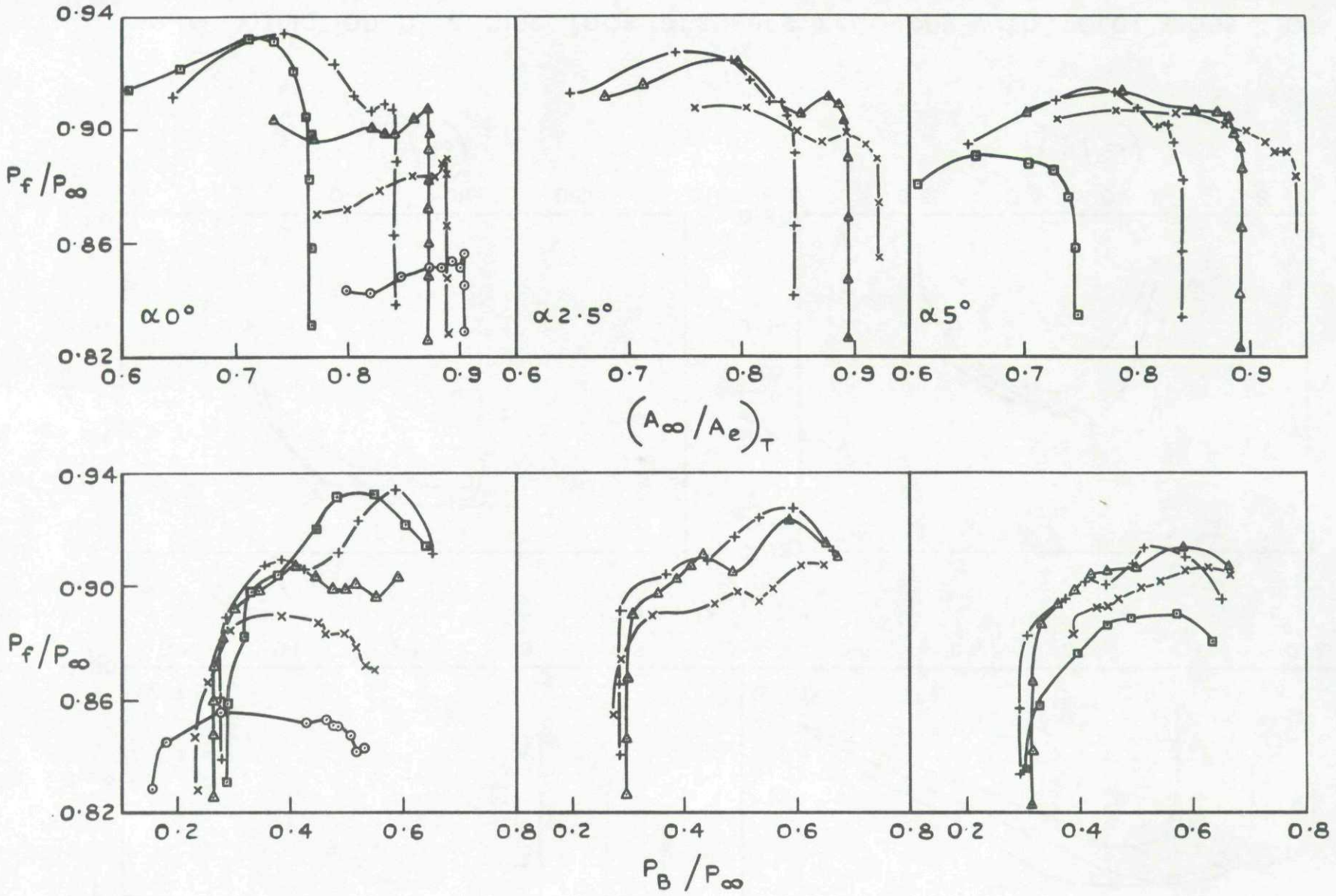

δ_2	2°	5°	7°	9°	12°
	⊙	×	△	+	⊡

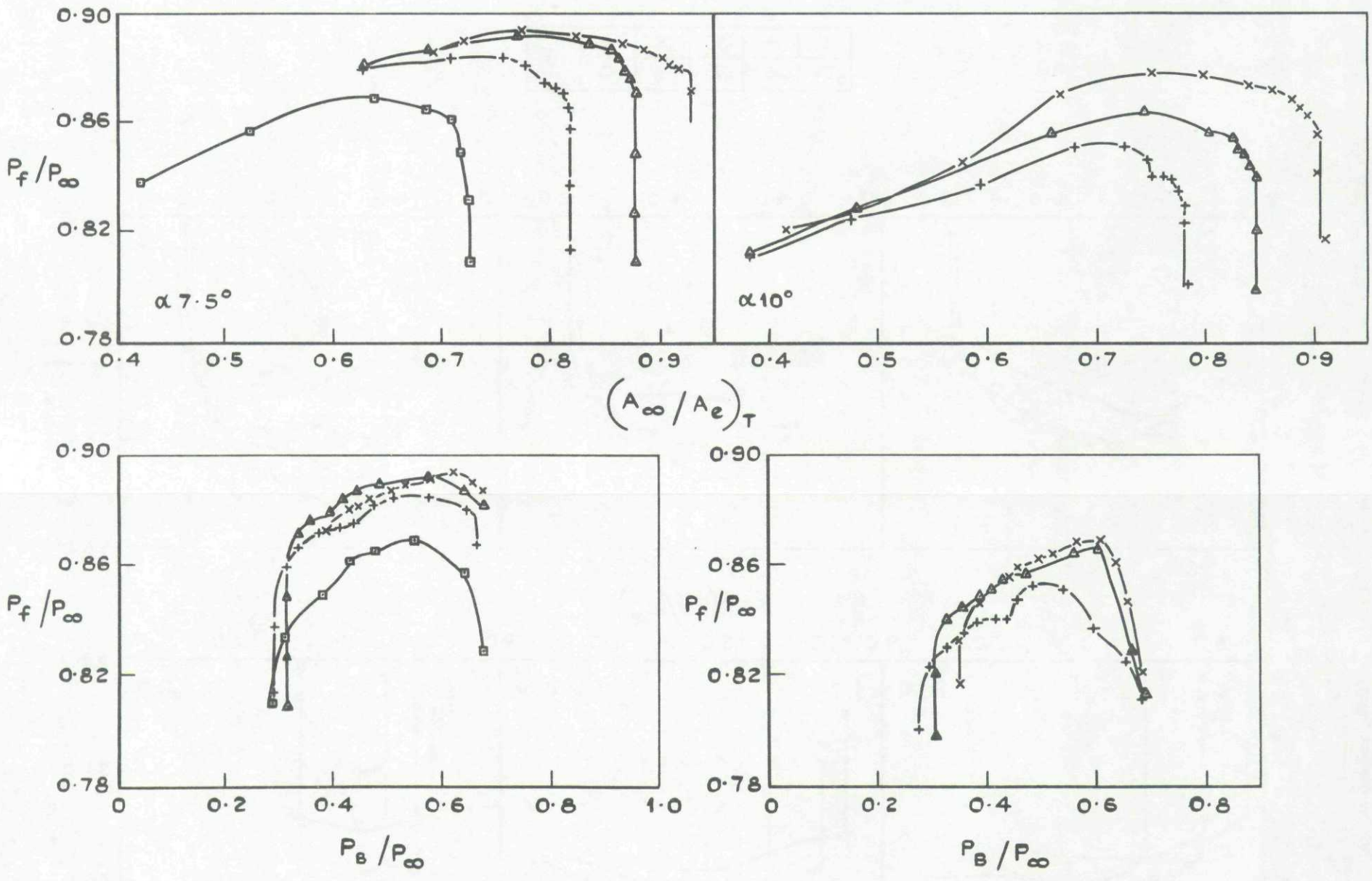

Fig. 13 Variation of engine face pressure recovery with total mass flow and with bleed pressure recovery
M_∞ 2·01 Bleed exit plug 4

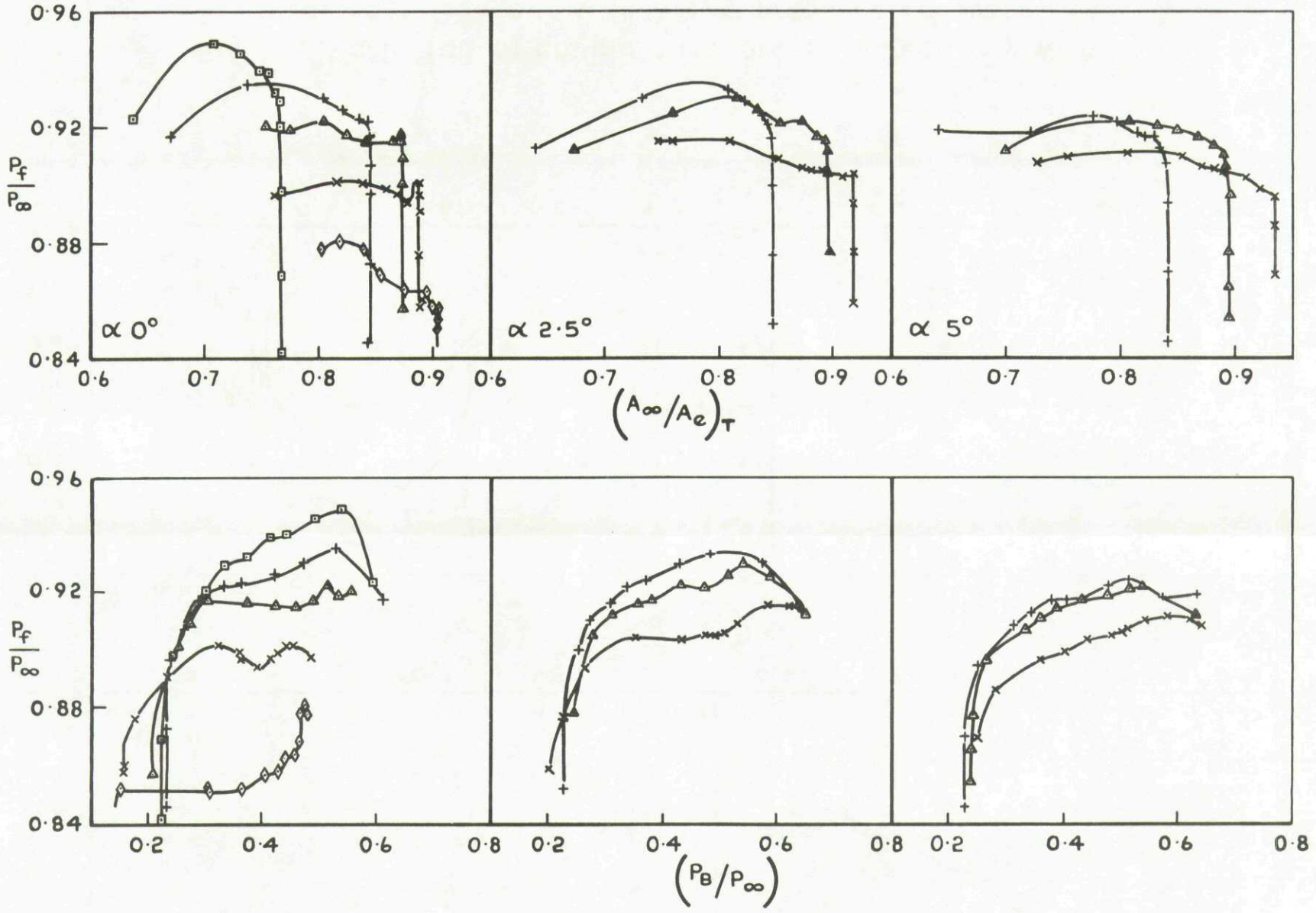

δ_2	0°	5°	7°	9°	12°
	◊	×	△	+	⊡

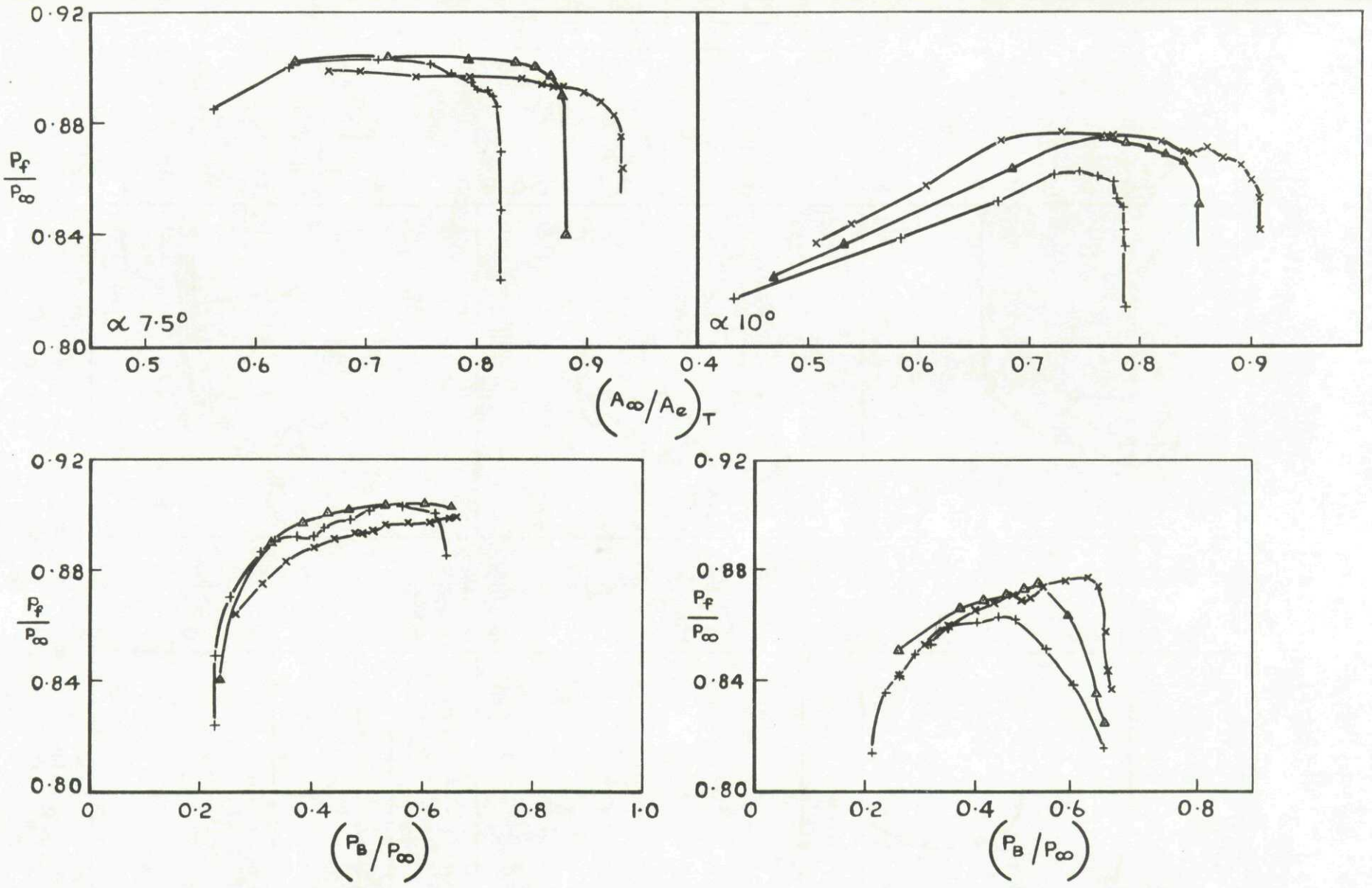

Fig.14 Variation of engine face pressure recovery with total mass flow and with bleed pressure recovery M_∞ 2·01. Bleed exit plug 8

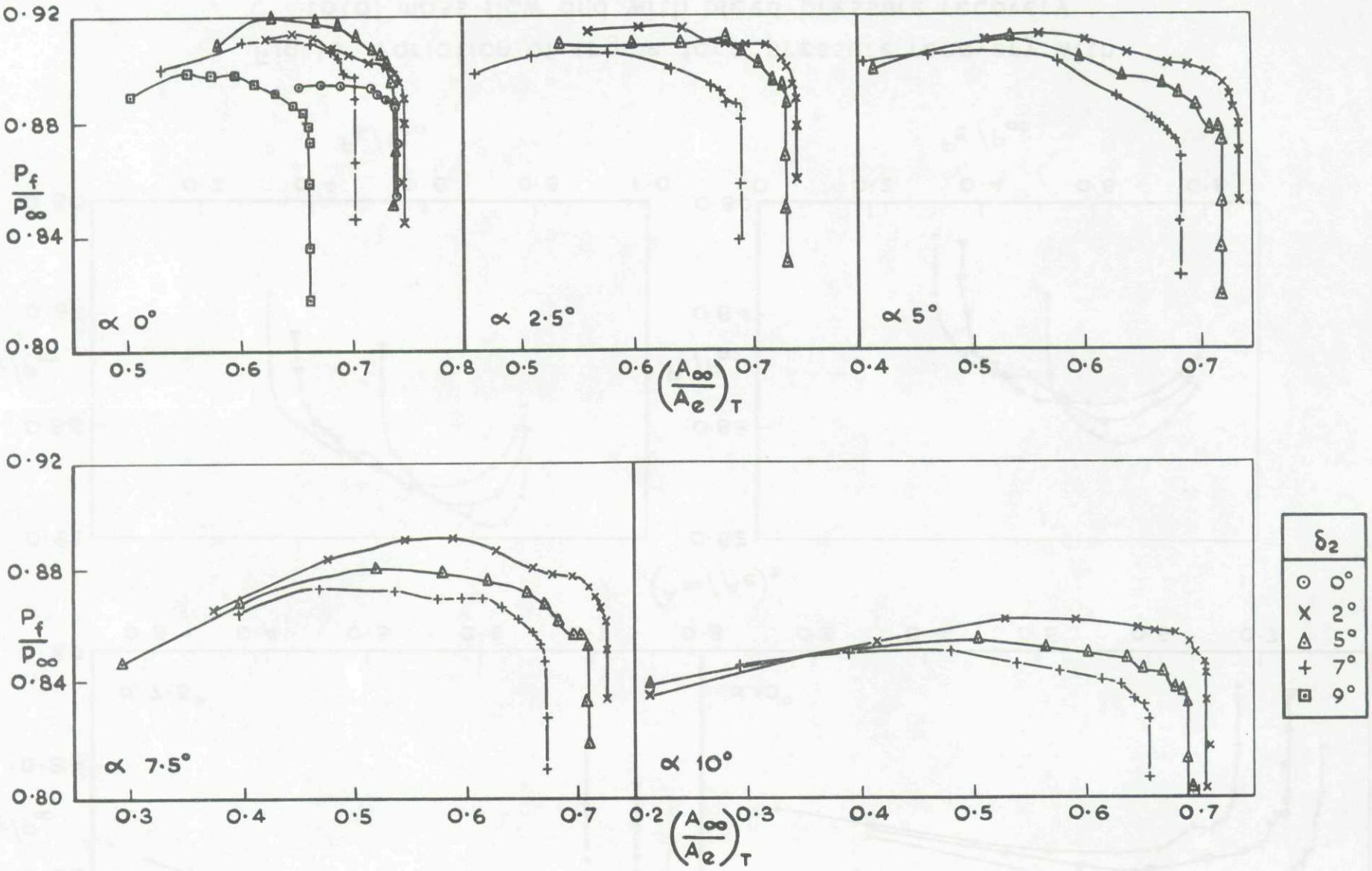

Fig.15 Variation of engine face pressure recovery with total mass flow.
M_∞ 1·70. Zero bleed

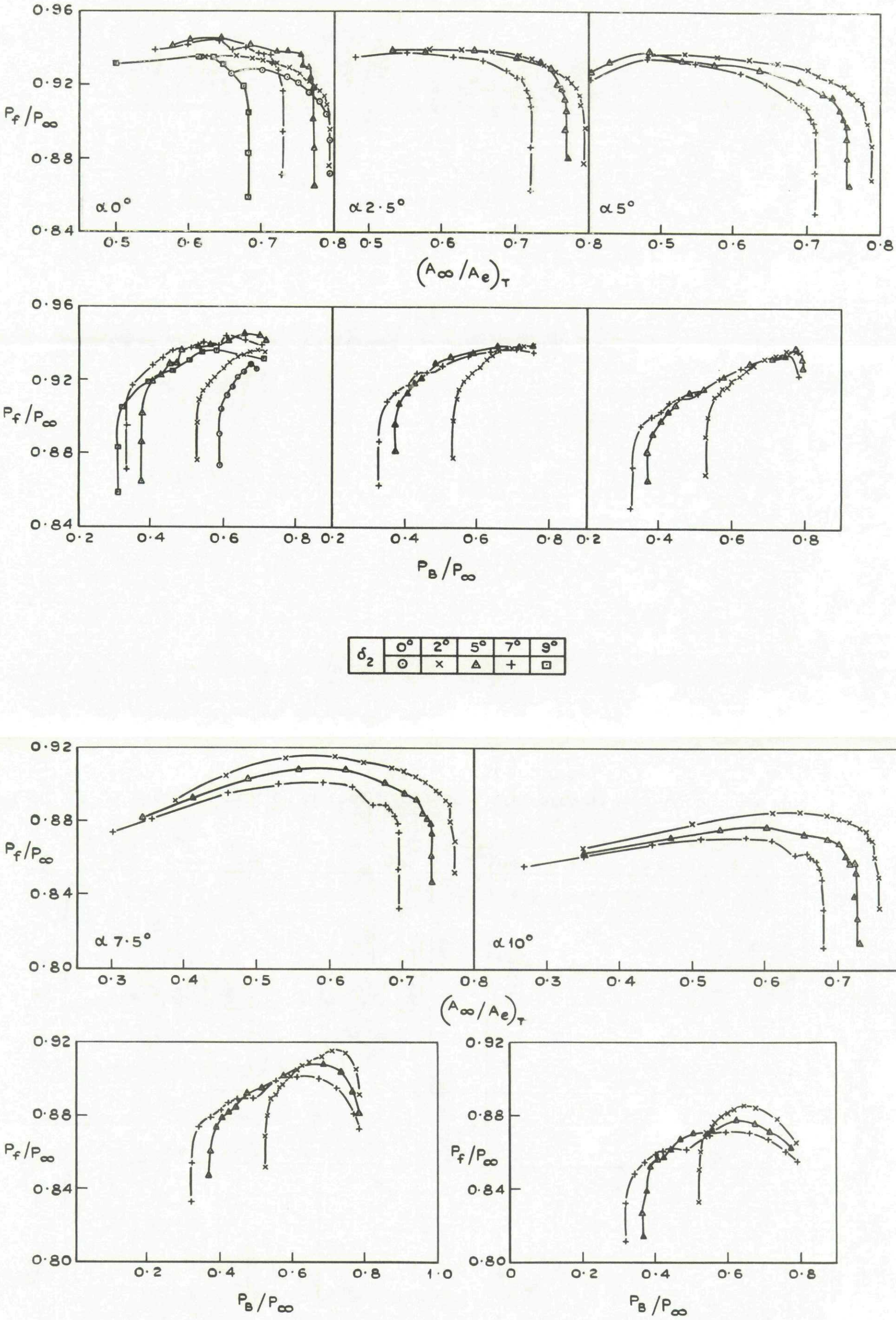

δ_2	0°	2°	5°	7°	9°
	⊙	×	△	+	⊡

Fig. 16 Variation of engine face pressure recovery with total mass flow and with bleed pressure recovery
M_∞ 1·70 Bleed exit plug 4

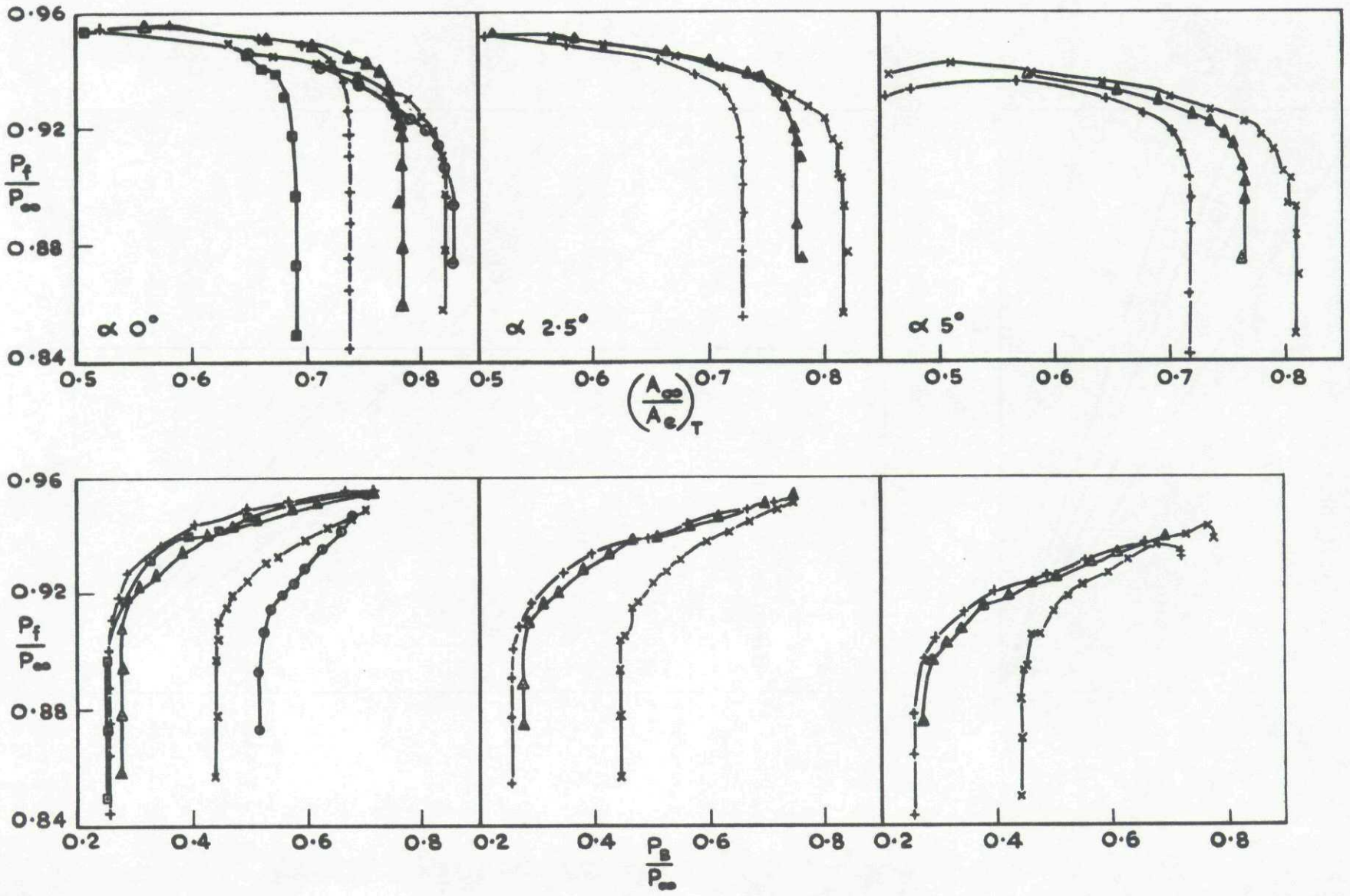

δ_2	0°	2°	5°	7°	9°
	⊙	×	△	+	⊡

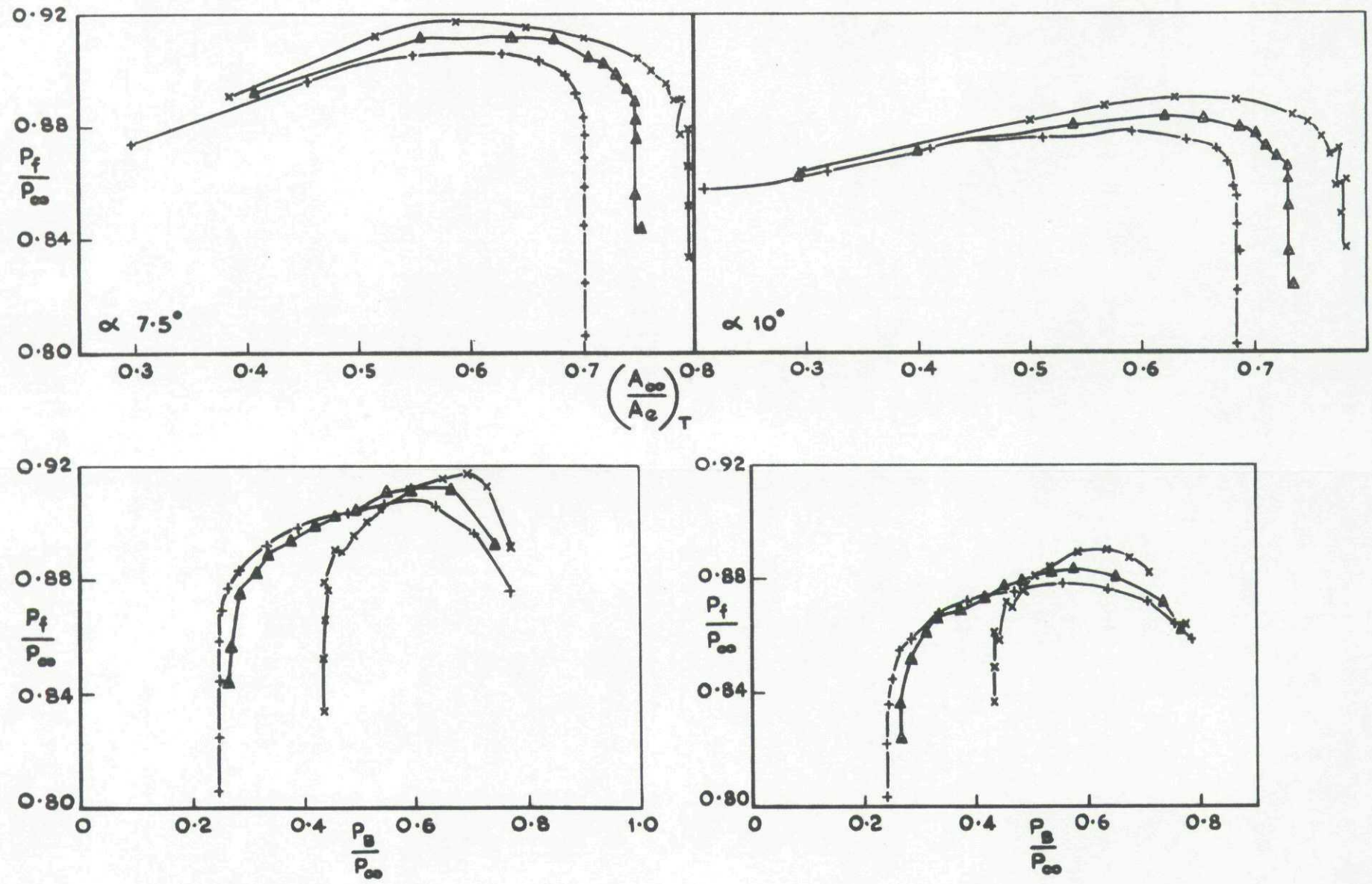

Fig.17 Variation of engine face pressure recovery with total mass flow and with bleed pressure recovery. M_∞ 1·70. Bleed exit plug 8

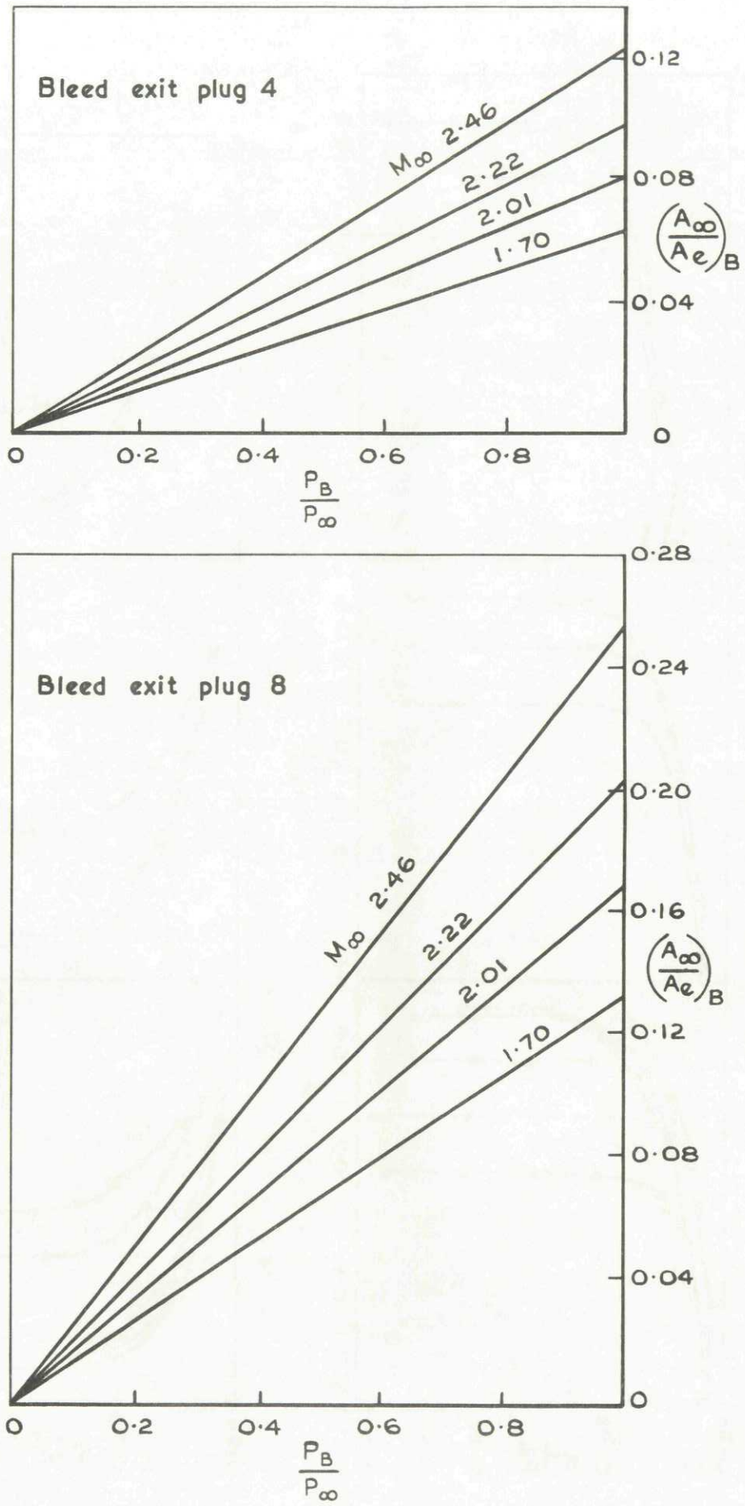

Fig.18 Relationship between bleed mass flow & bleed pressure recovery

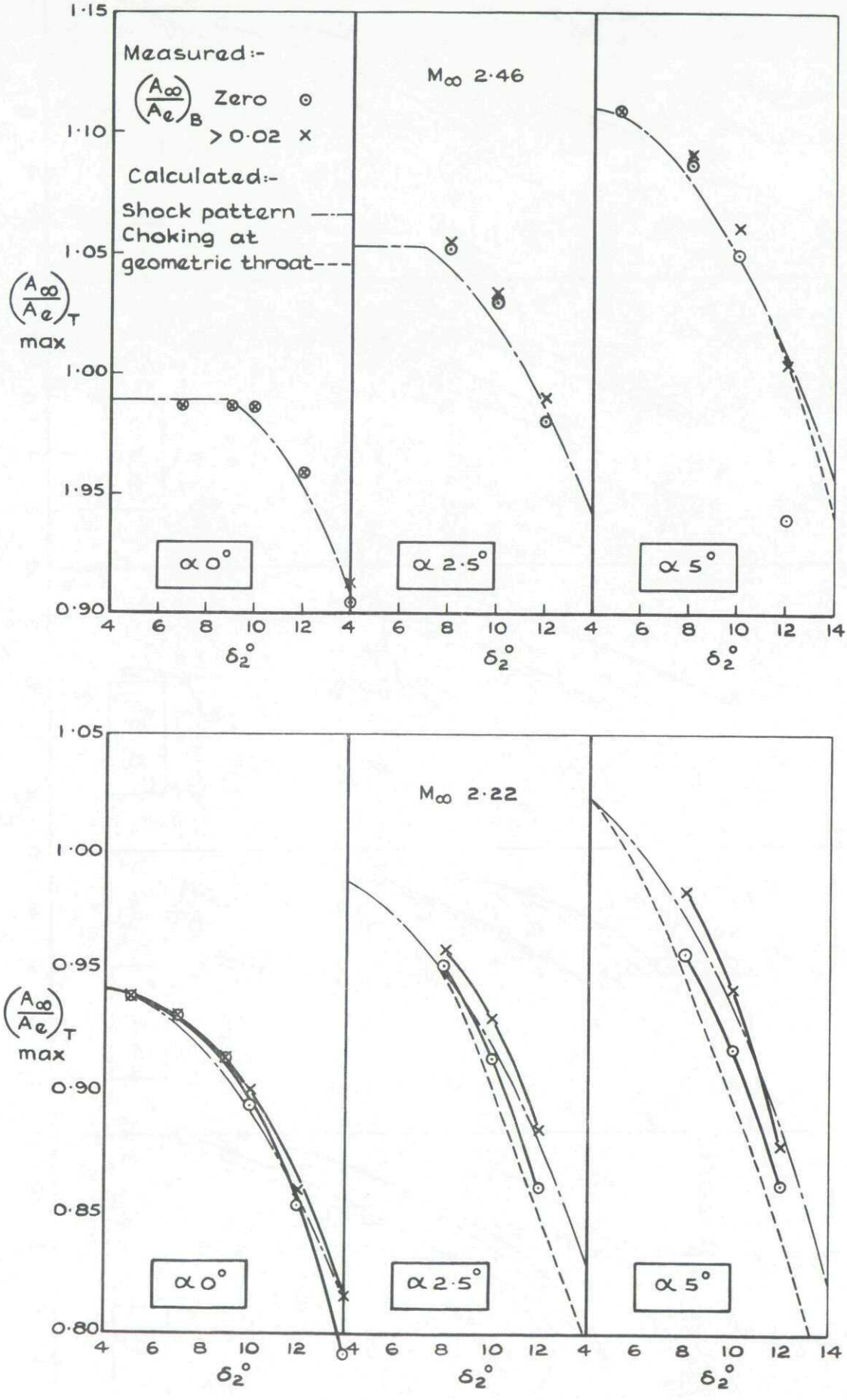

Fig.19 Variation of maximum total mass flow with second ramp angle. M_∞ 2·22 & 2·46

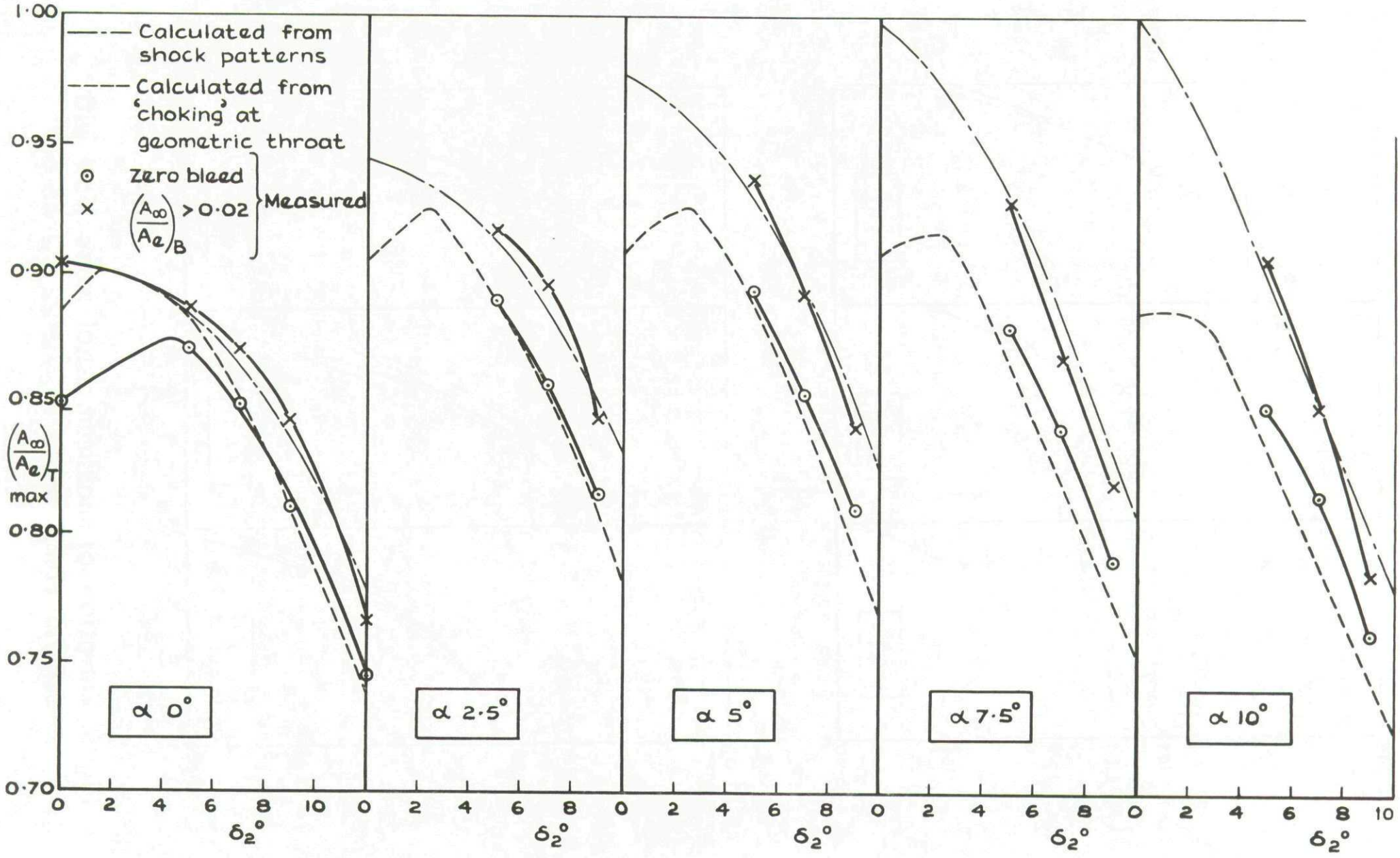

Fig.20 Variation of maximum total mass flow with second ramp angle M_∞ 2·01

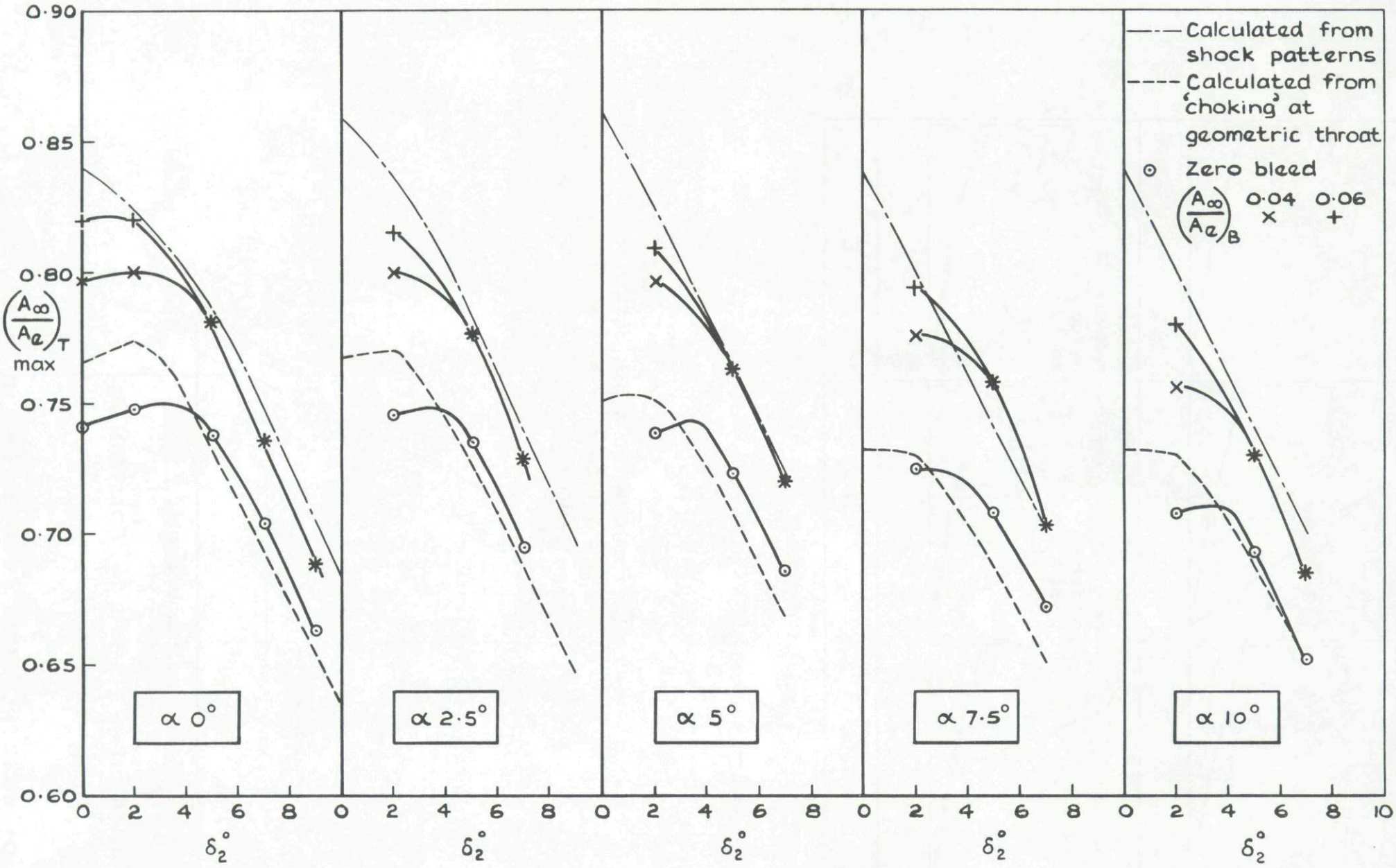

Fig. 21 Variation of maximum total mass flow with second ramp angle. M_∞ 1·70

Theoretical shock patterns appropriate to the particular regions A, B, C, D & E

Shock patterns assumed for the purpose of estimating maximum mass flow

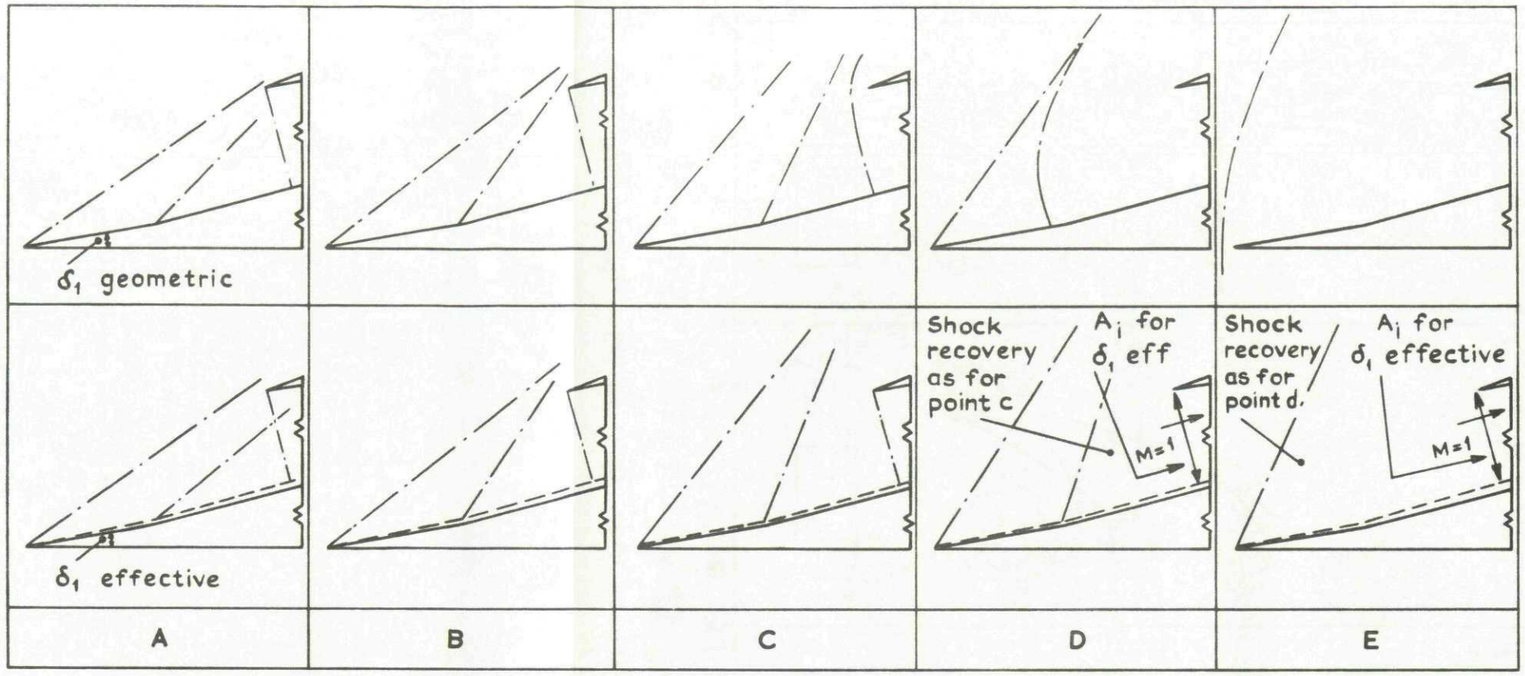

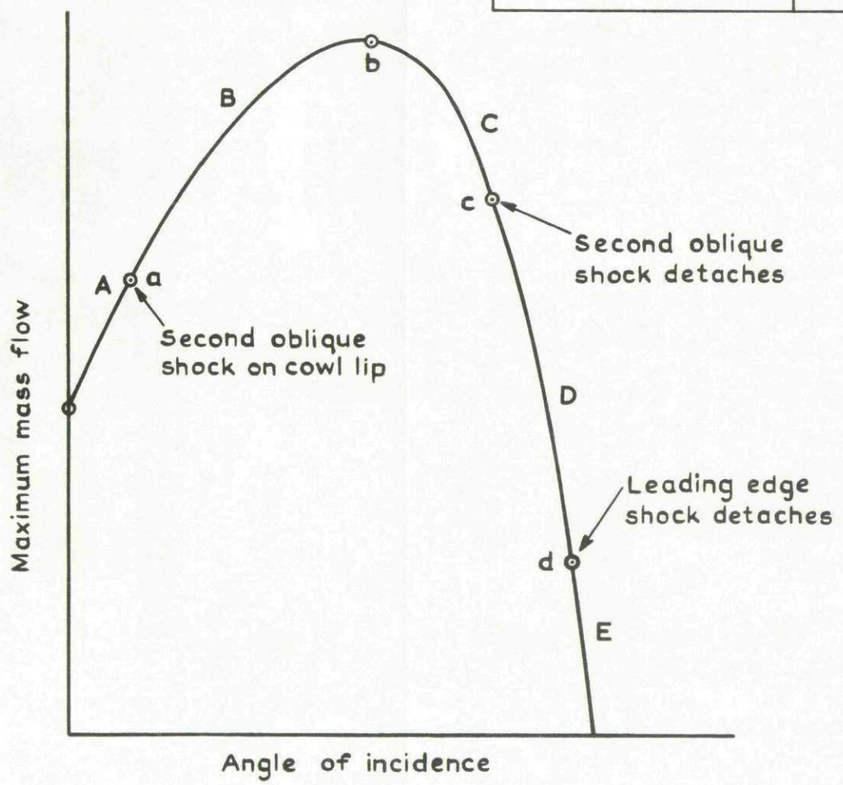

Variation of $\left(\frac{A_\infty}{A_e}\right)_{max}$ with α. Constant M_∞, δ_1 & δ_2

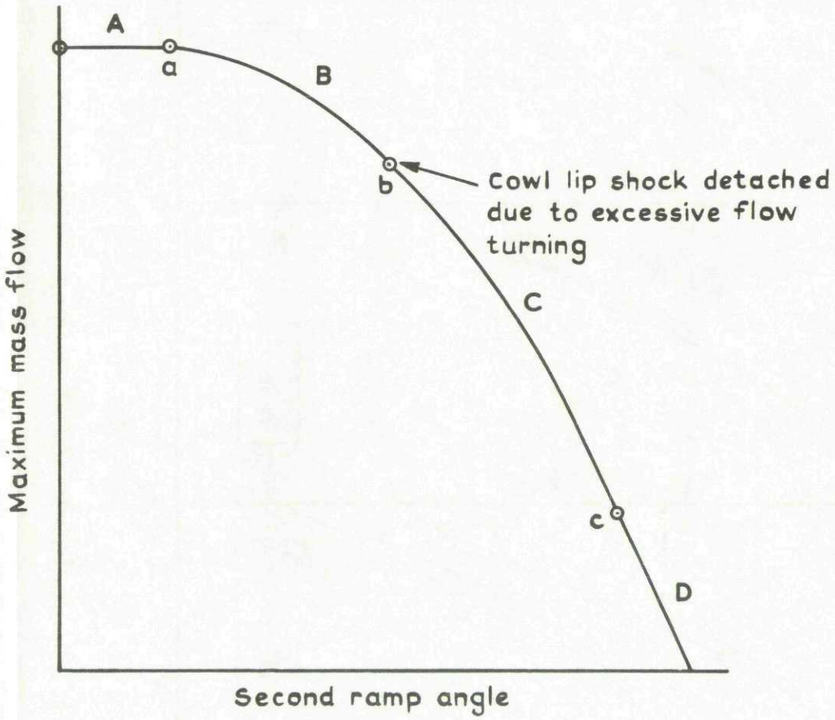

Variation of $\left(\frac{A_\infty}{A_e}\right)_{max}$ with δ_2. Constant M_∞, δ_1 & α

Fig. 22 Variation of maximum mass flow with angle of incidence and second ramp angle

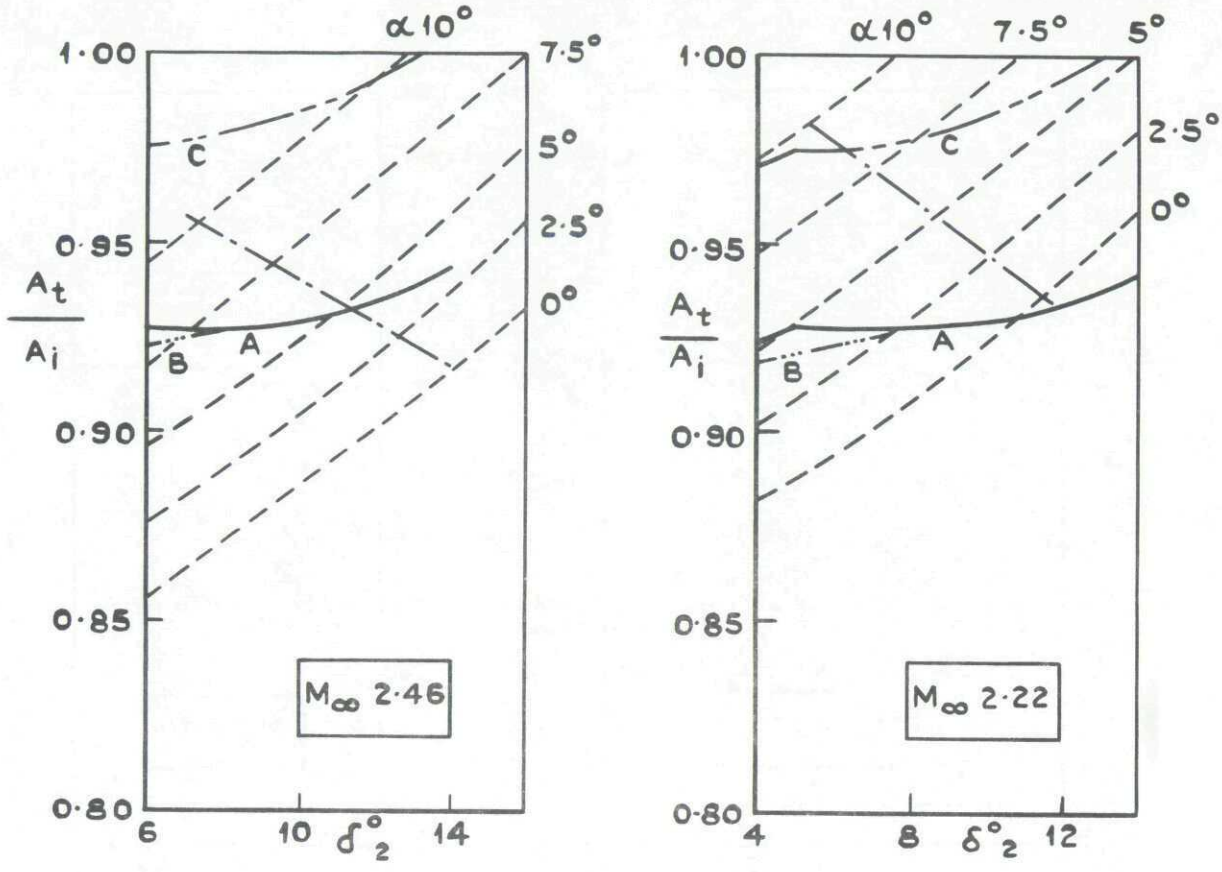

– – – – – One dimensional area ratio required for starting the internal flow

Curve A ——— Ratio A_t (geometric) to A_i $(\delta_1 = 10^\circ)$

Curve B —·····— Ratio A_t (effective) to A_i $(\delta_1 = 11^\circ)$ at zero bleed

Curve C —·—·— Ratio A_t (geometric) to A_i $(\delta_i = 11^\circ)$

—·—·—·— Limit of δ_2 beyond which shock detachment takes place at cowl lip due to excessive flow turning

Fig. 23 a Comparison of the internal contraction of the intake with the area ratios required for starting. M_∞ 2·22 & 2·46

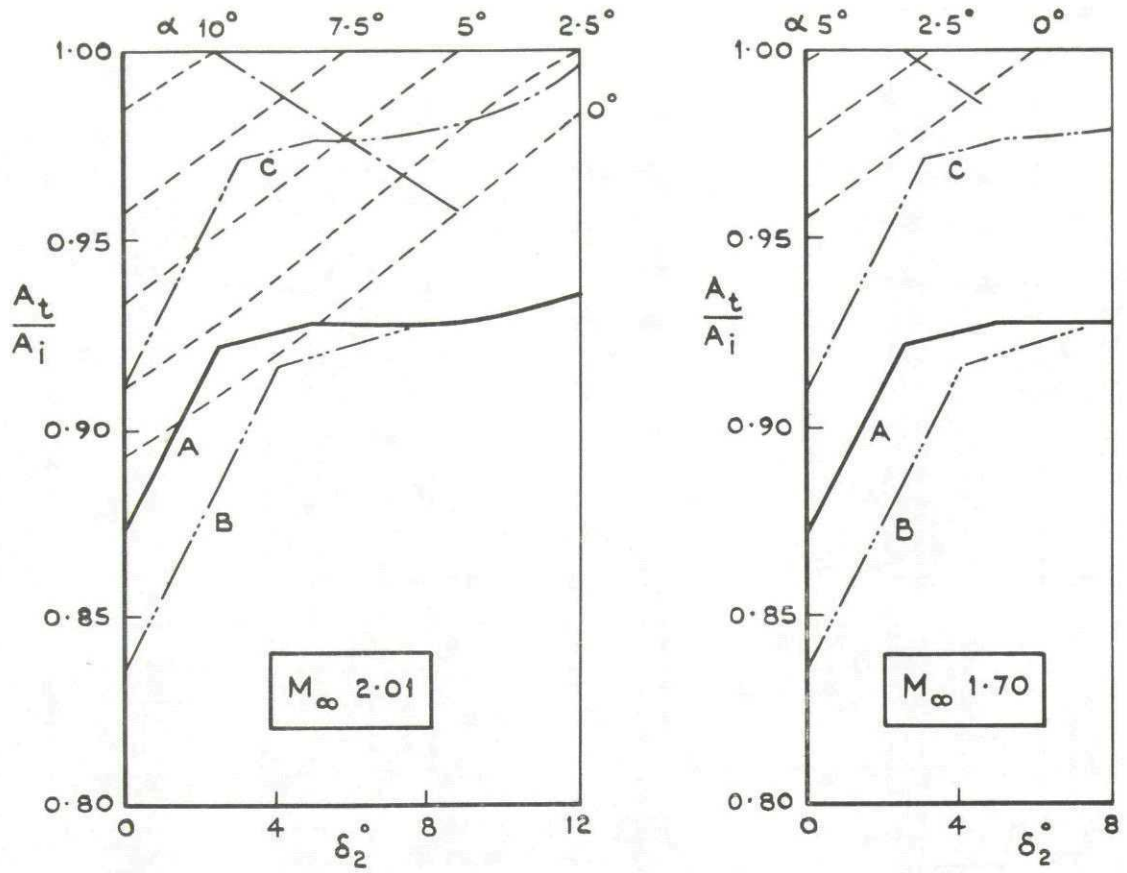

– – – – – One dimensional area ratio required for starting the internal flow

Curve A ——— Ratio A_t (geometric) to A_i ($\delta_1 = 10°$)

Curve B —·—·— Ratio A_t (effective) to A_i ($\delta_1 = 11°$) at zero bleed

Curve C —··—··— Ratio A_t (geometric) to A_i ($\delta_1 = 11°$)

—·—·— Limit of δ_2 beyond which shock detachment takes place at cowl lip due to excessive flow turning

Fig. 23 b Comparison of the internal contraction of the intake with the area ratios required for starting M_∞ 2·01 & 1·70

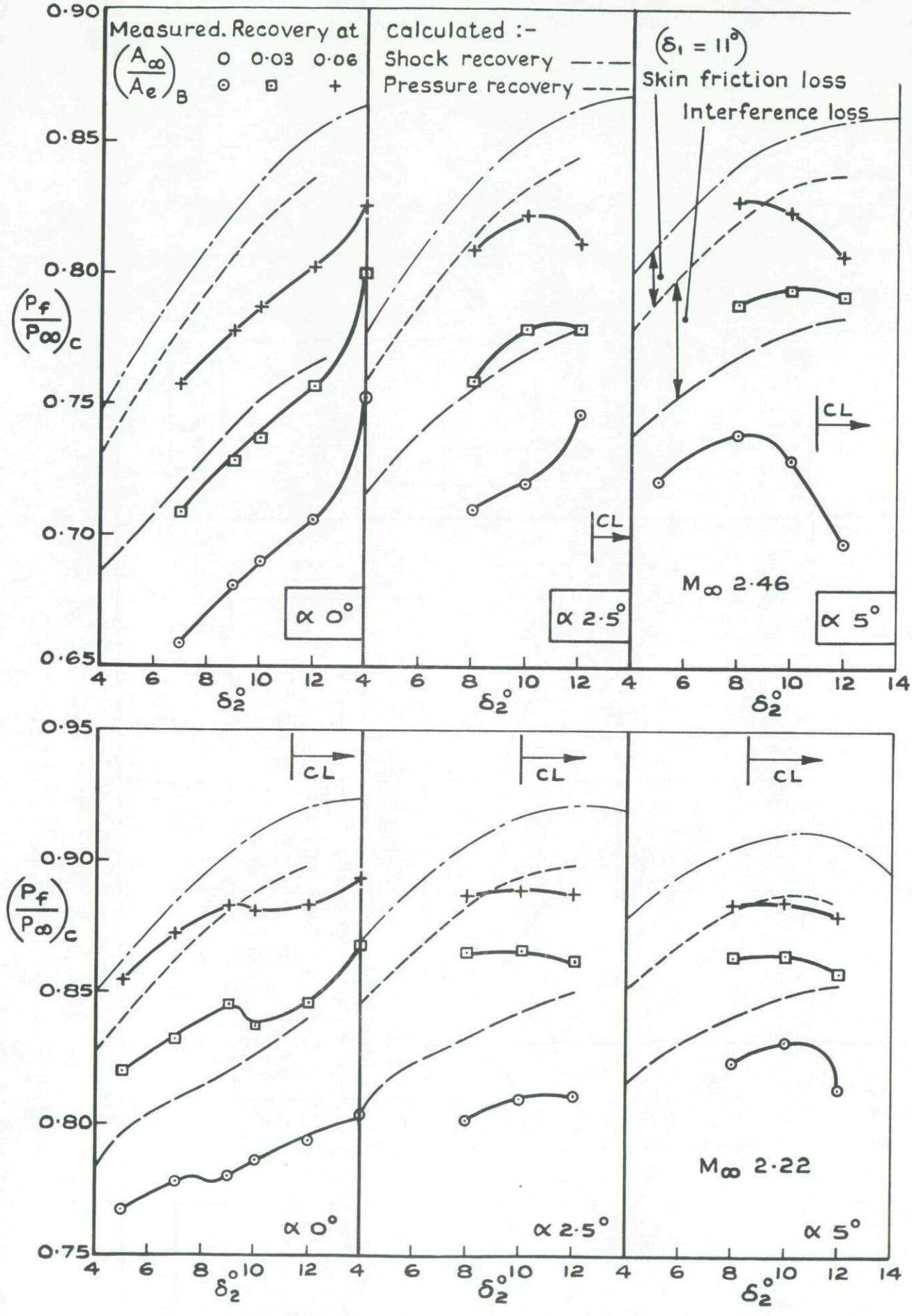

Fig. 24 Variation of critical point pressure recovery with second ramp angle.

M_∞ 2·46 & 2·22

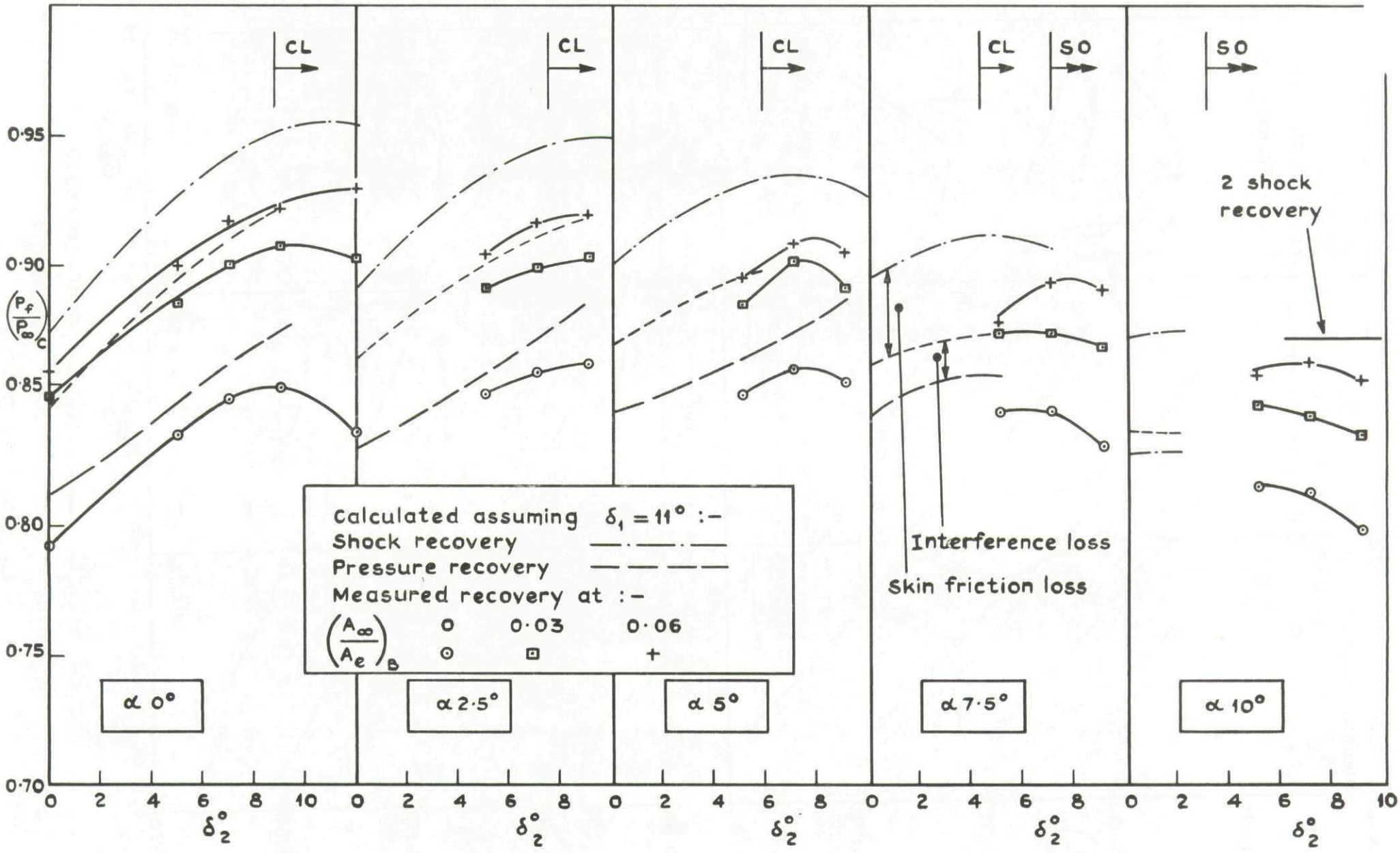

Fig.25 Variation of critical point pressure recovery with second ramp angle : M_∞ 2·01

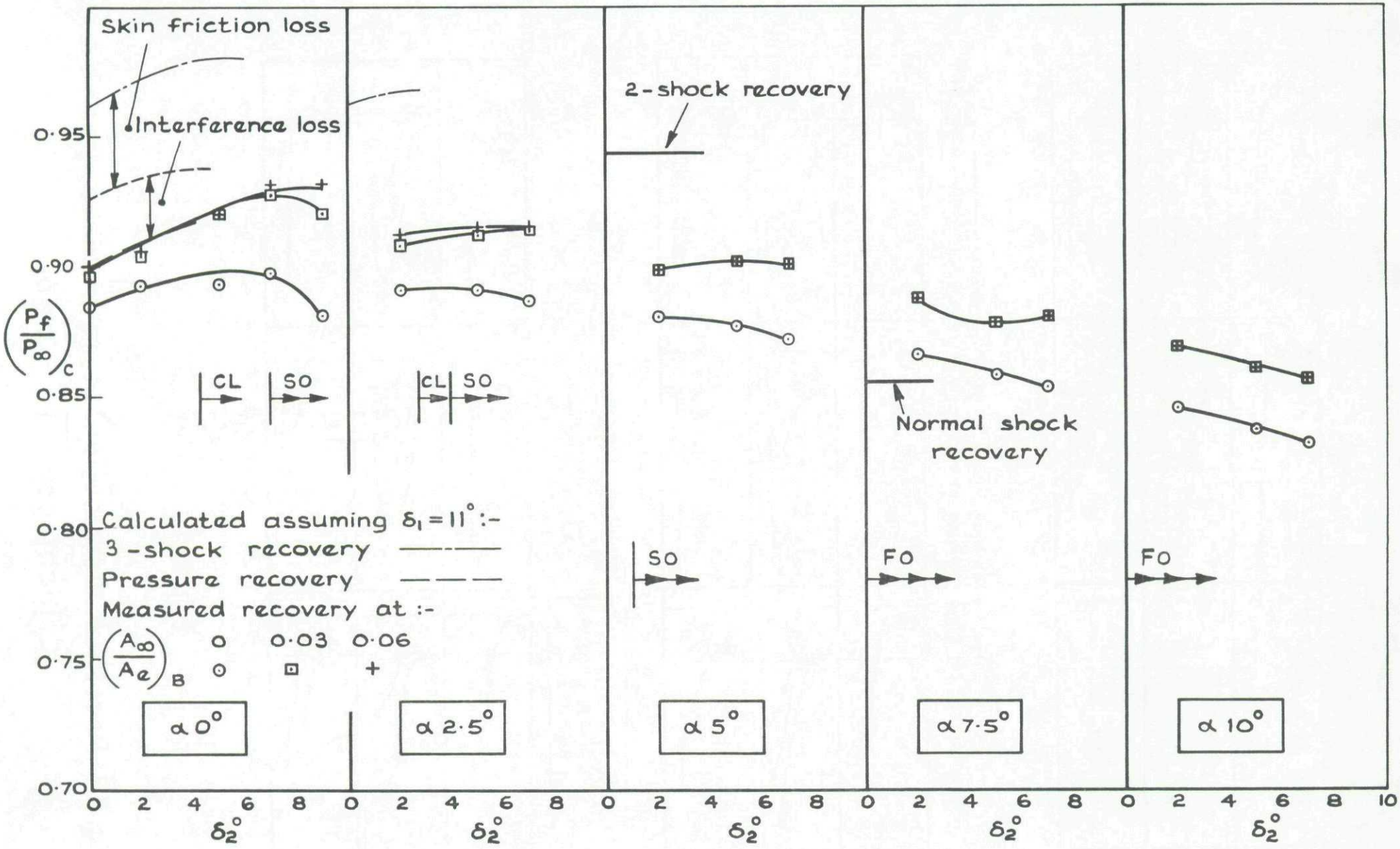

Fig. 26 Variation of critical point pressure recovery with second ramp angle. M_∞ 1·70

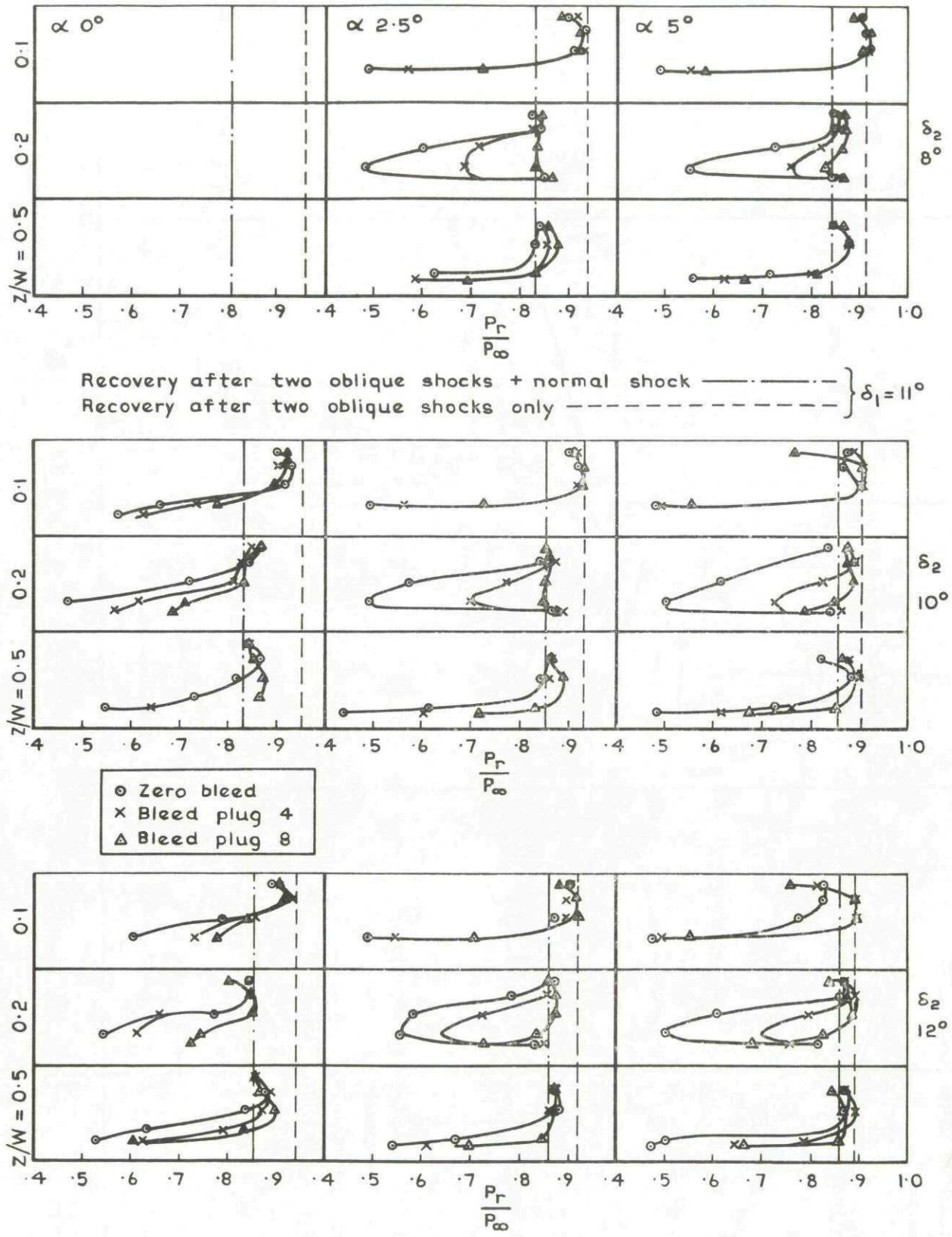

Fig. 27 Pressure distribution at rear hinge position.
Critical point M_∞ 2·46

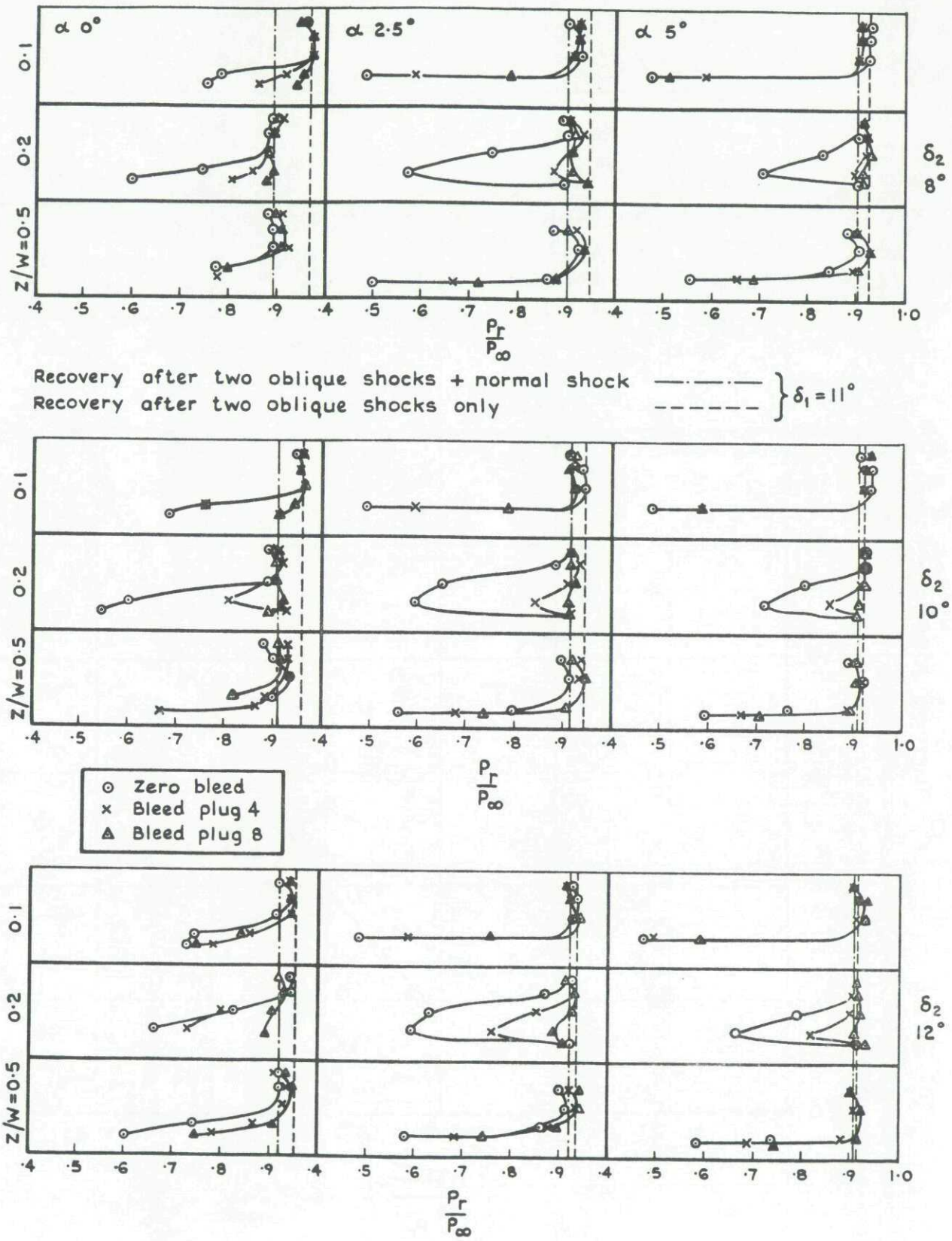

Fig. 28 Pressure distribution at rear hinge position
Critical point M_∞ 2·22

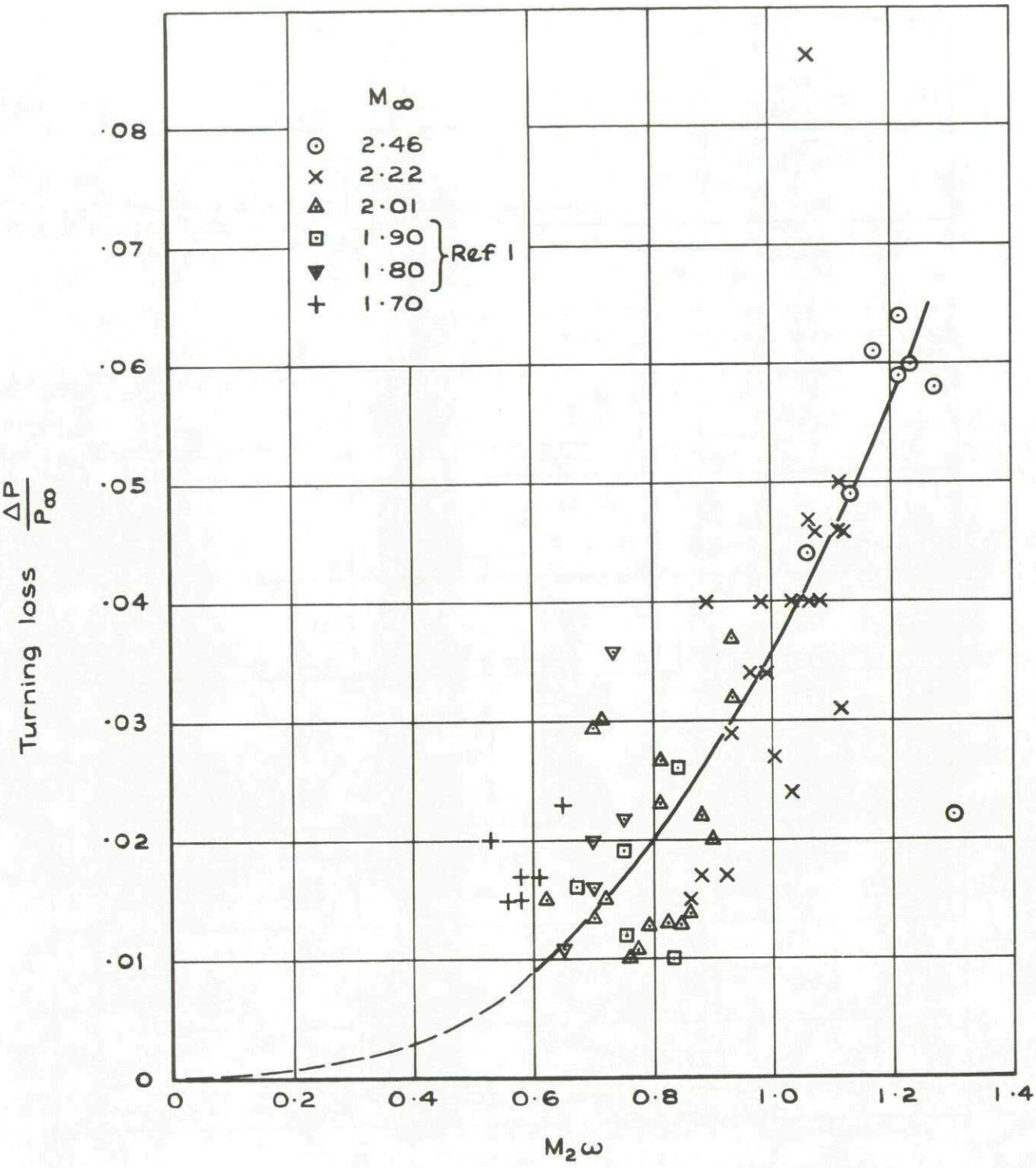

Fig. 29 Correlation of flow turning loss with normal shock Mach number & angle between front & rear movable ramps

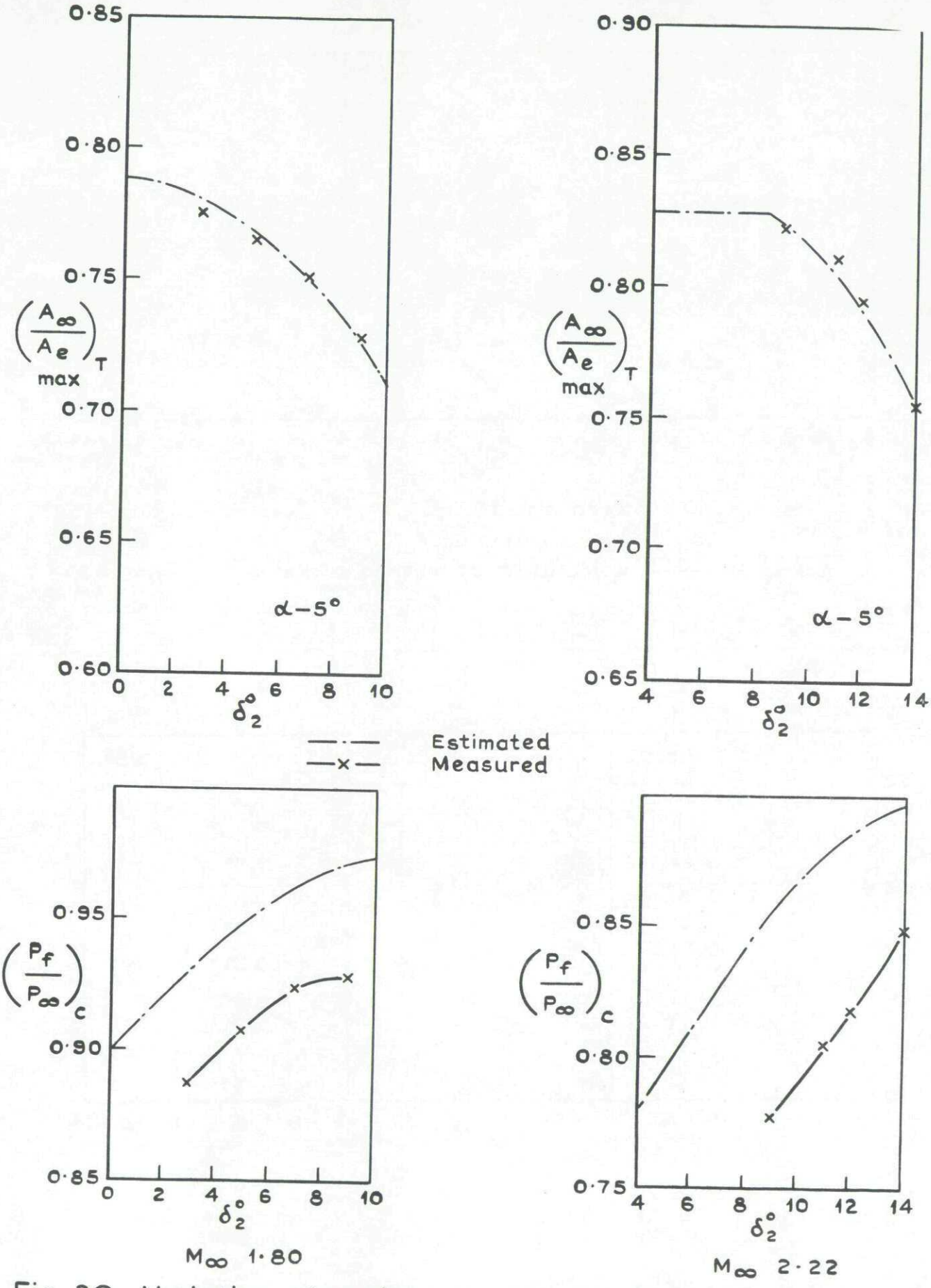

Fig. 30 Variation of maximum total mass flow and critical point pressure recovery with δ_2. Constant bleed exit area : plug No. 4 negative incidence : $\alpha - 5^\circ$ M_∞ 1·80 & 2·22

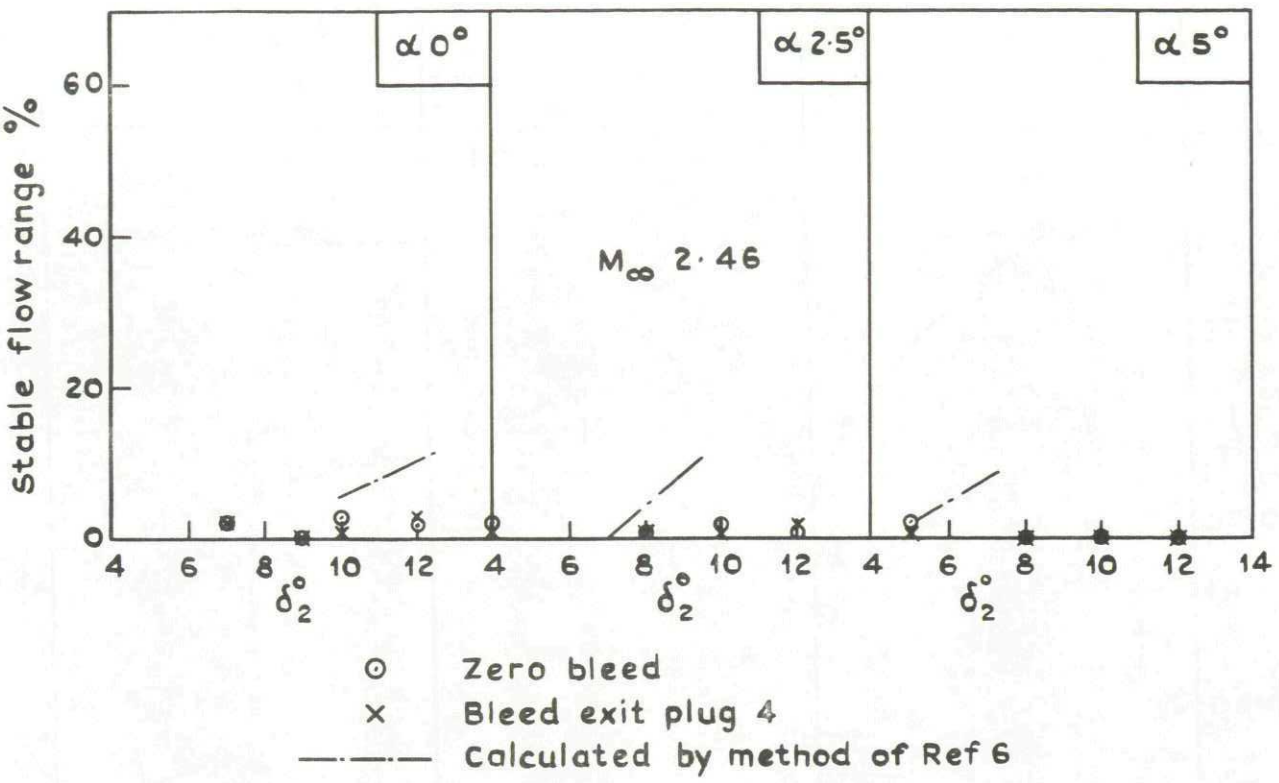

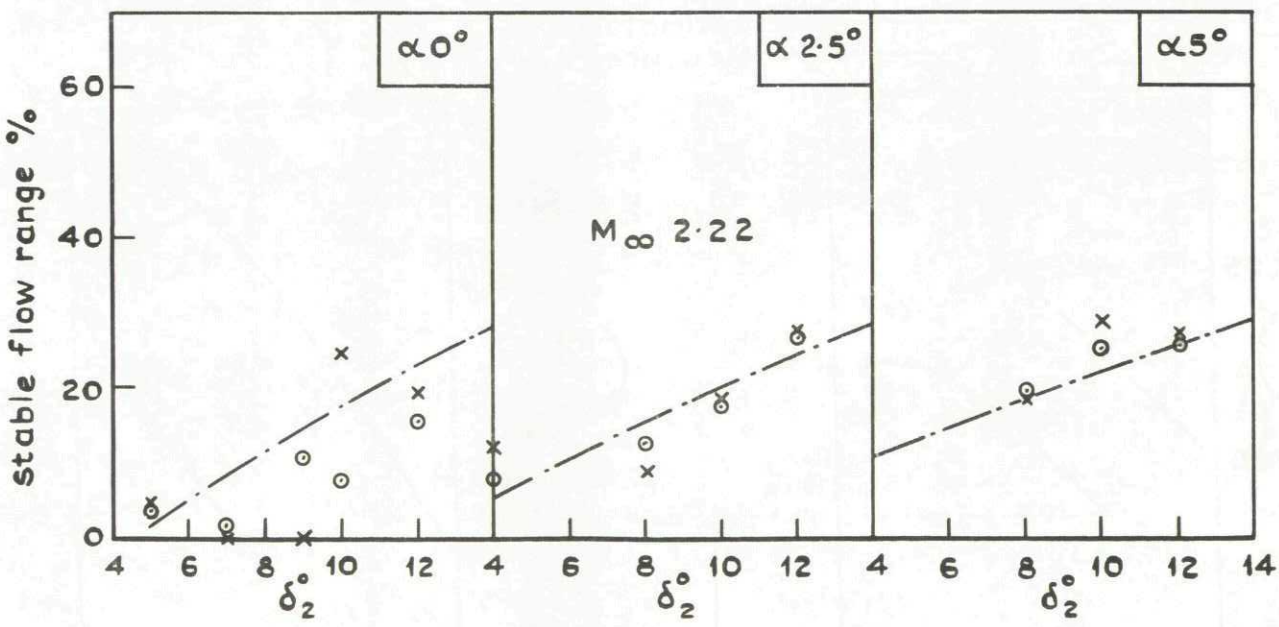

Fig. 31 Variation of stable flow range with δ_2. M_∞ 2·46 & 2·22

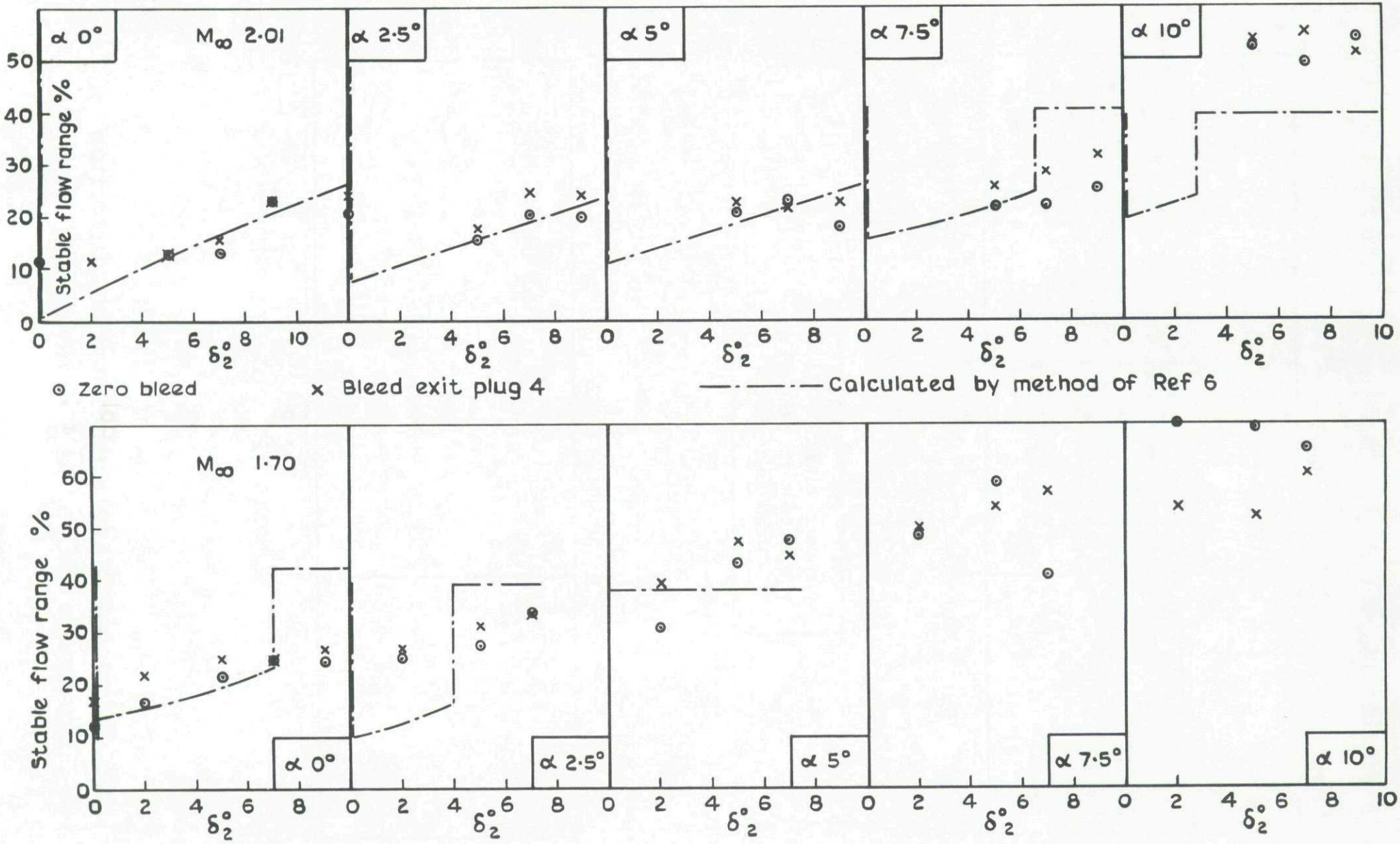

Fig.32 Variation of stable flow range with δ_2. M_∞ 2·01 & 1·70

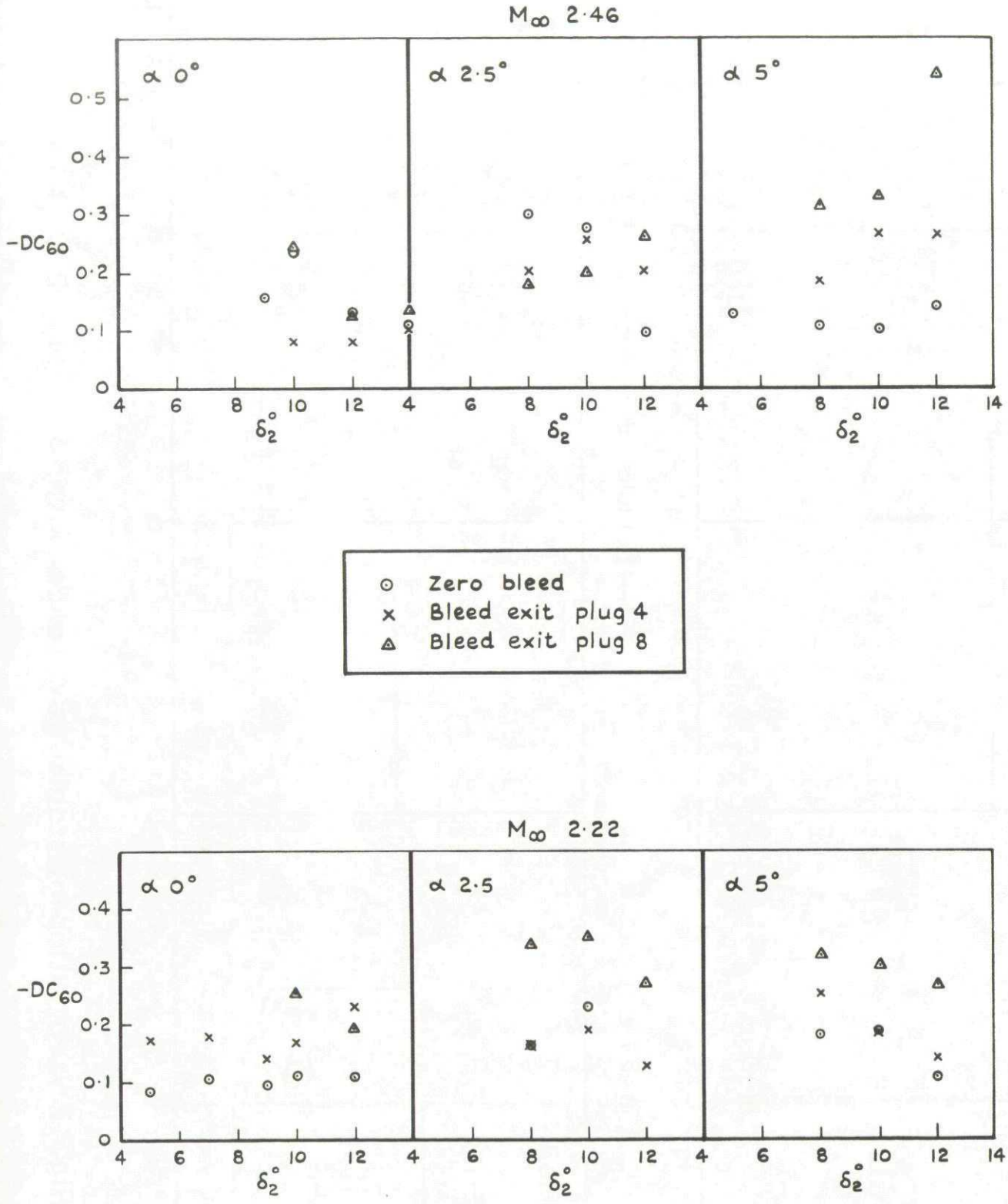

Fig. 33 Effect of bleed & incidence on distortion parameter DC_{60} M_∞ 2·46 & 2·22

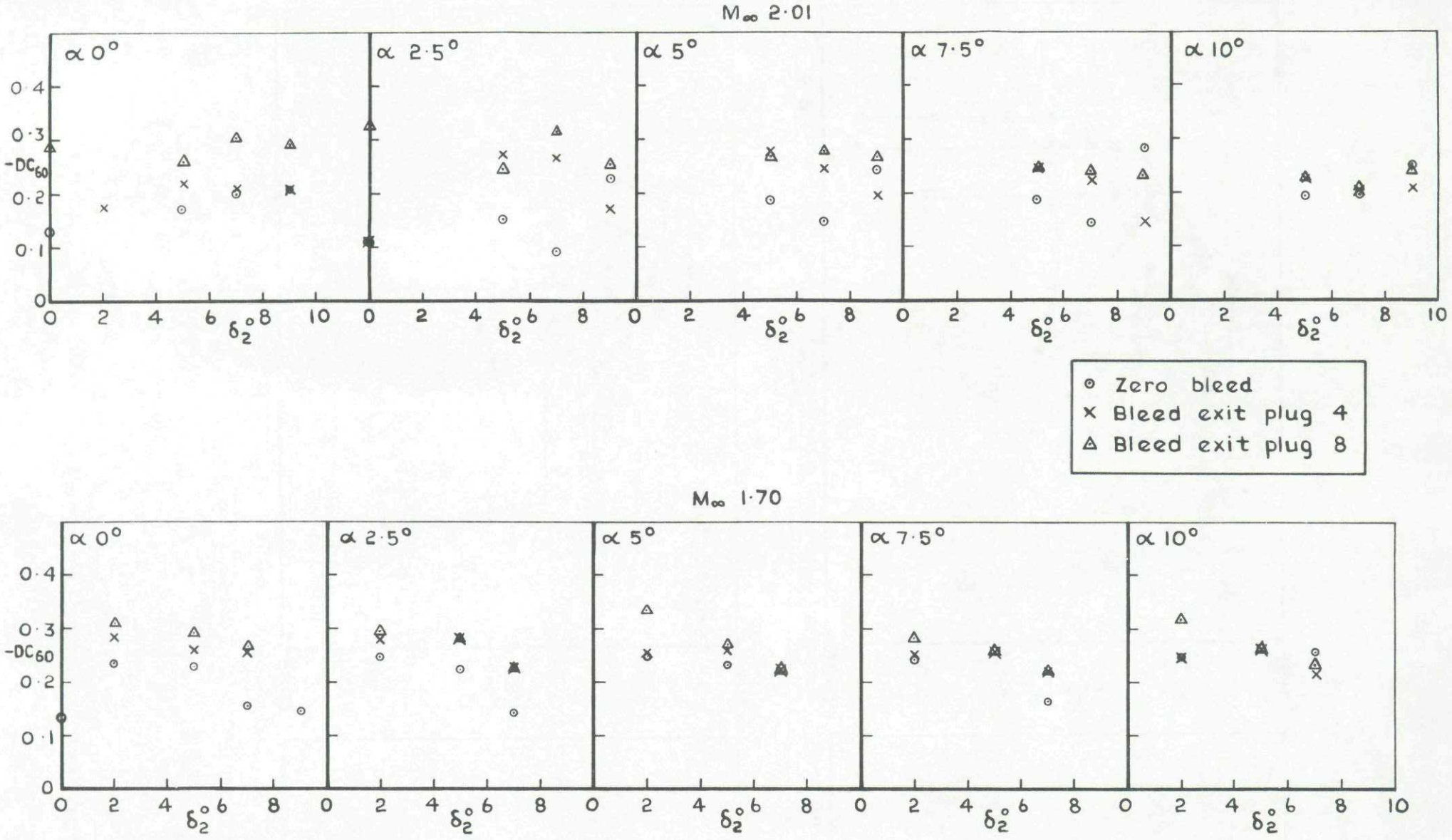

Fig. 34 Effect of bleed & incidence on distortion parameter DC_{60}
M_∞ 2·01 & 1·70

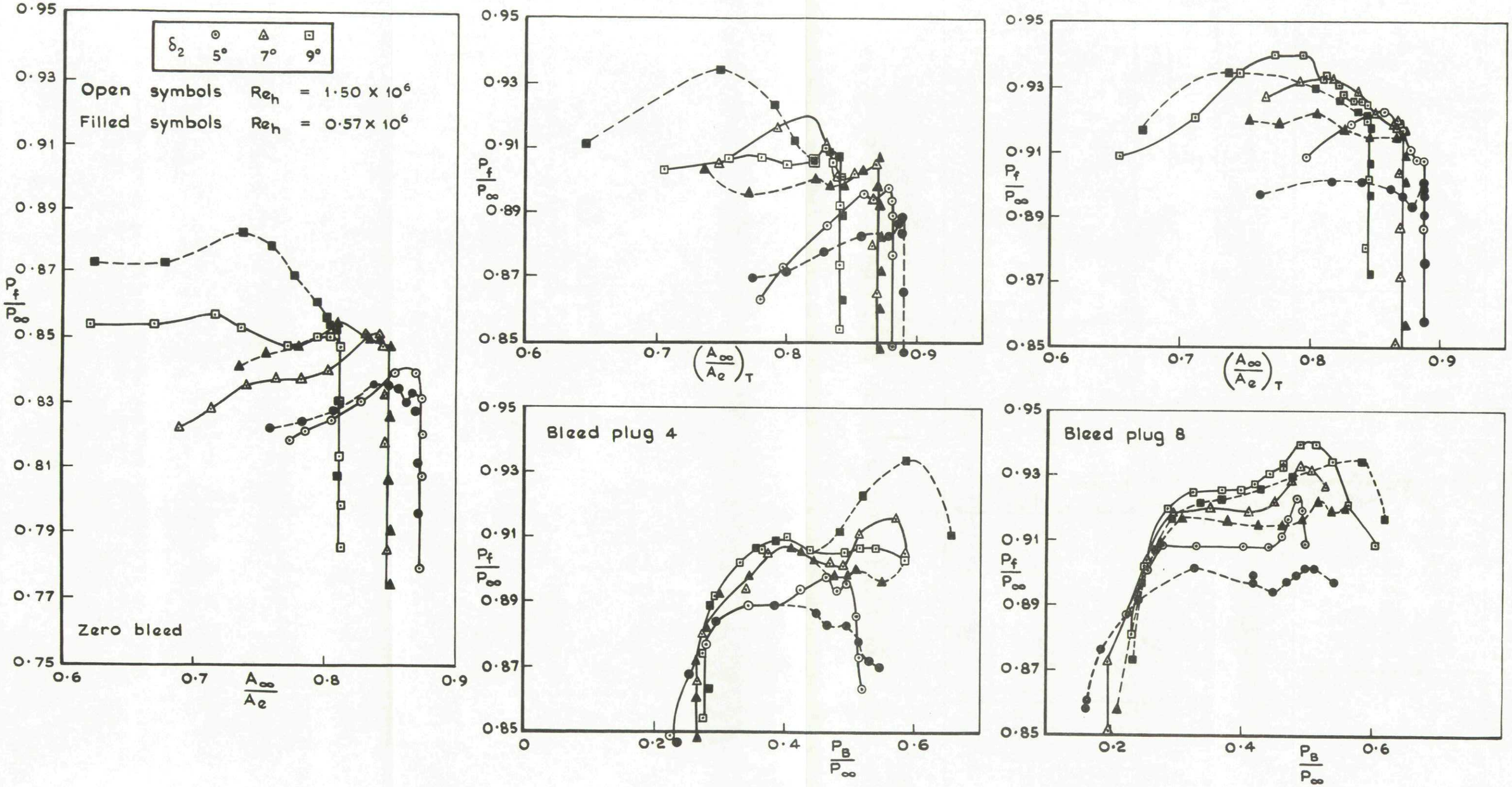

Fig. 35 Effect of Reynolds number on pressure recovery characteristics

M_∞ 2·01 α 0°

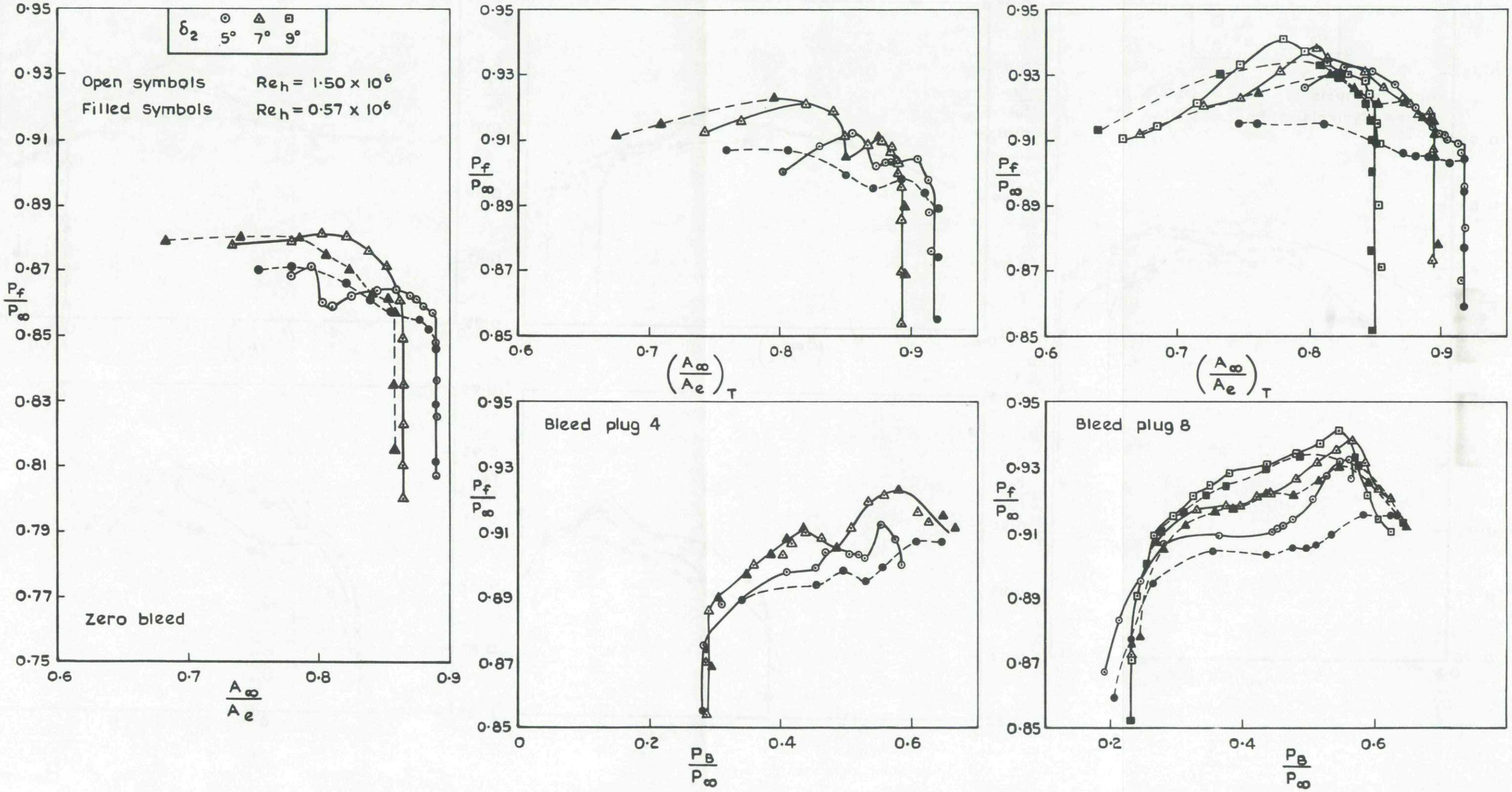

Fig.36 Effect of Reynolds number on pressure recovery characteristics.
M_∞ 2·01 α 2·5°

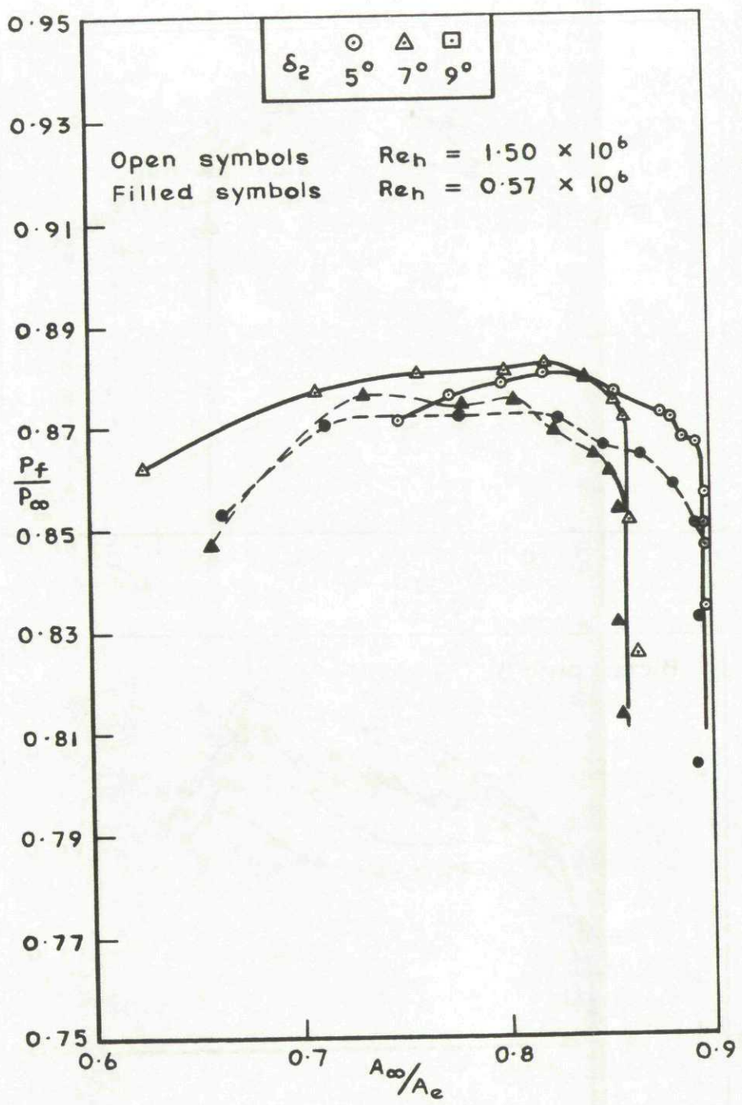

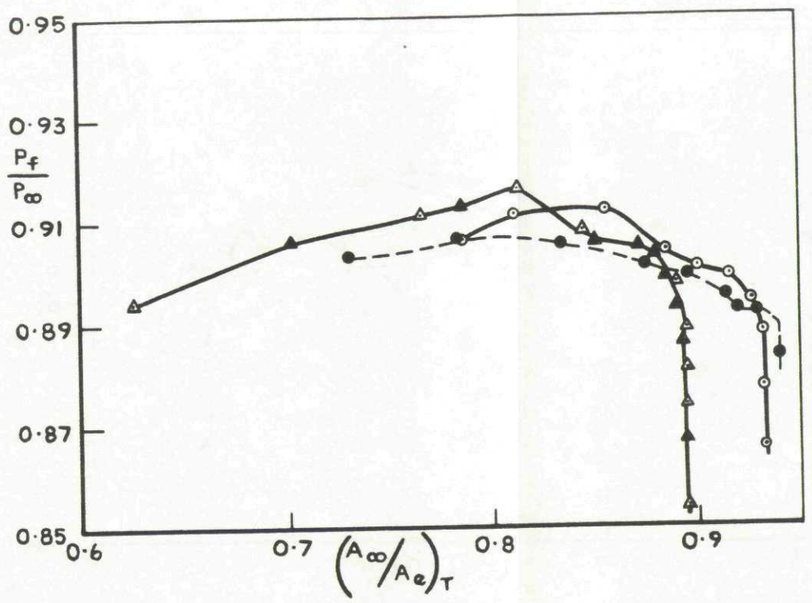

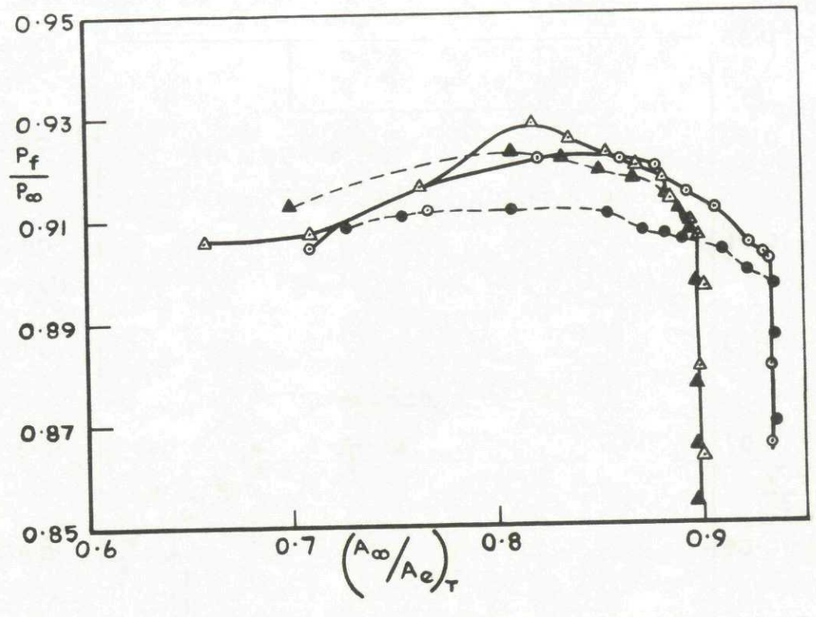

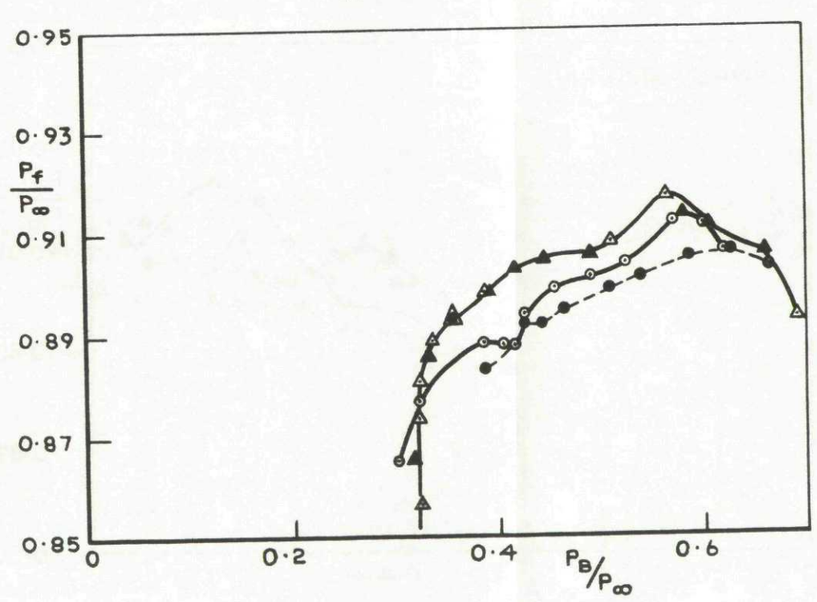

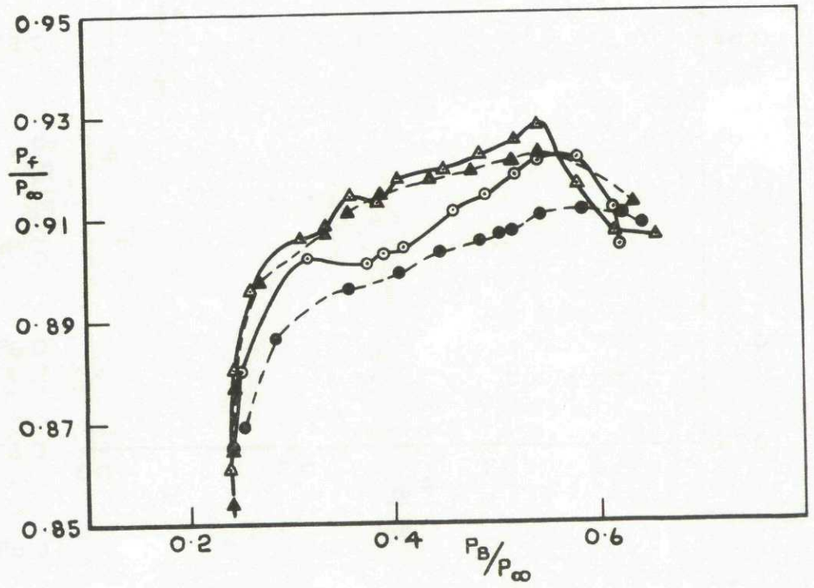

Fig. 37 Effect of Reynolds number on pressure recovery characteristics
M_∞ 2·01 α 5°

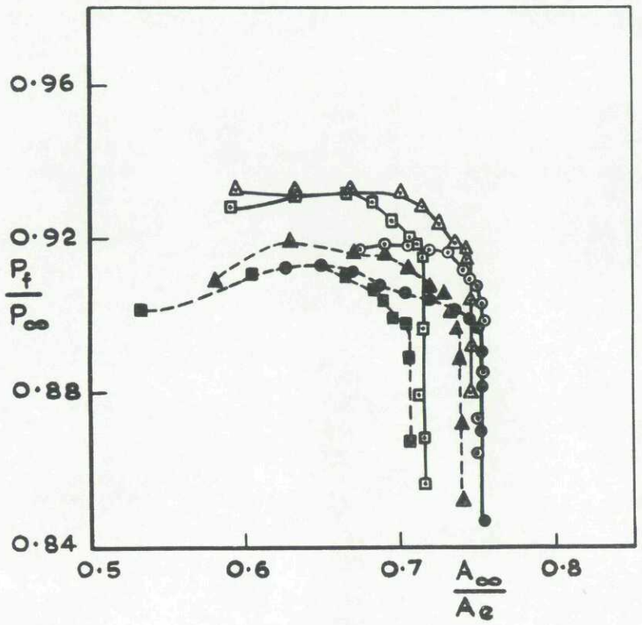

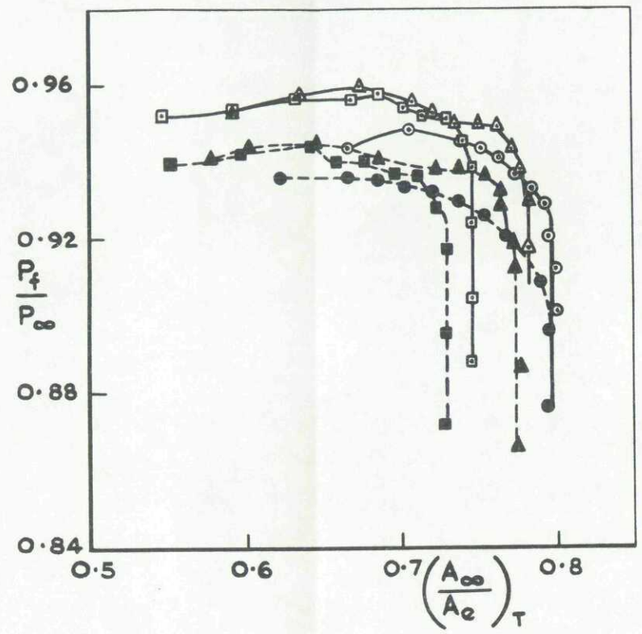

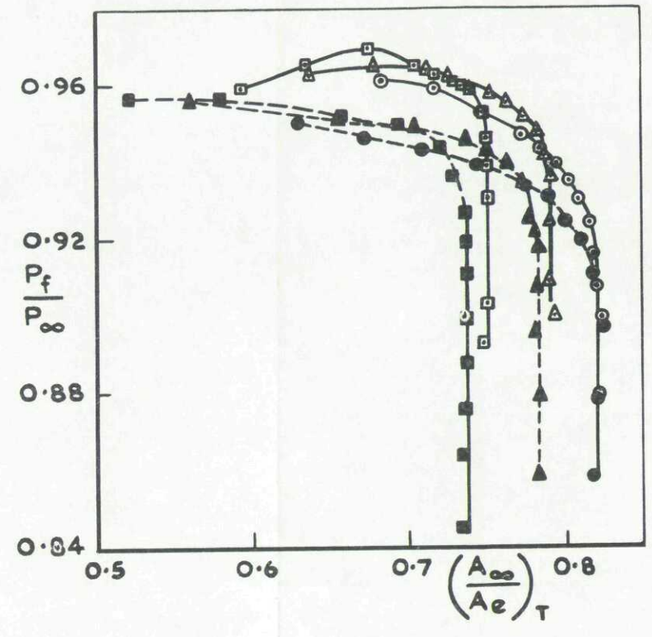

δ_2	⊙	△	⊡
	2°	5°	7°

Open symbols Re_h $1{\cdot}54 \times 10^6$

Filled symbols Re_h $0{\cdot}69 \times 10^6$

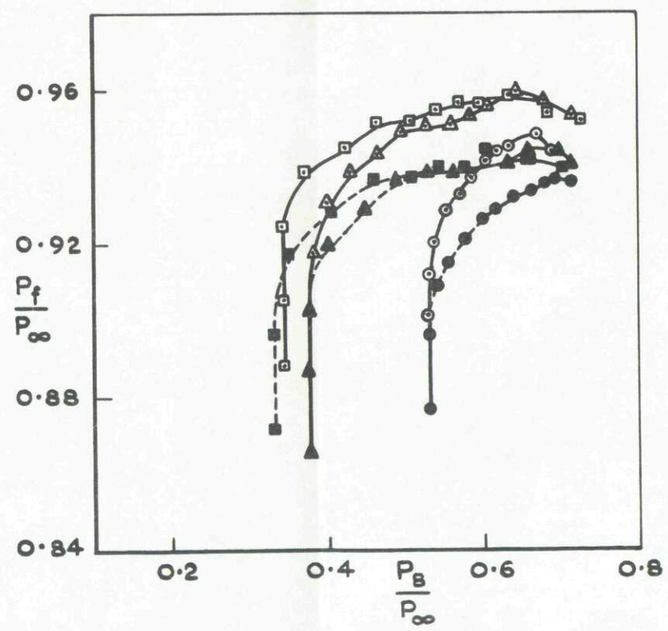

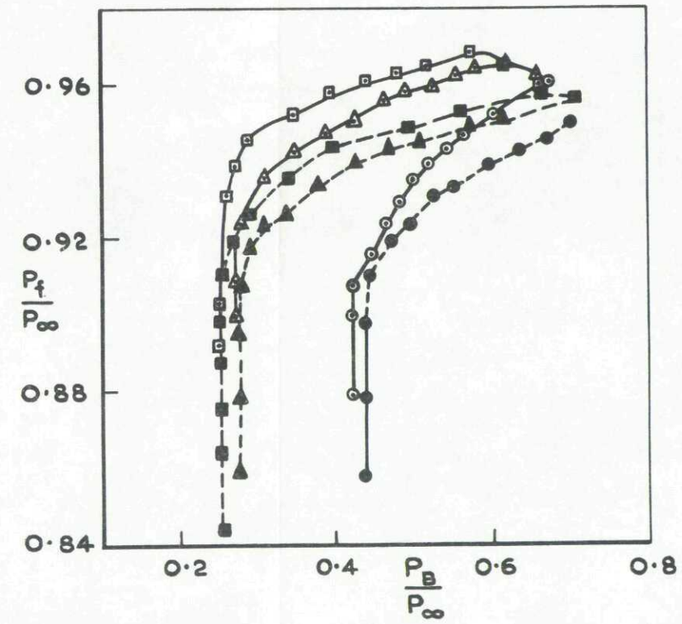

Fig. 38 Effect of Reynolds number on pressure recovery characteristics

M_∞ 1·70 α 0°

Printed in England for Her Majesty's Stationery Office by the Royal Aircraft Establishment, Farnborough. Dd 503427 K4 1/73

ARC CP No.1242
December 1971

533.697.2 :
533.6.015 :
533.6.011.5

Brown, C. S.
Goldsmith, E. L.

MEASUREMENT OF THE INTERNAL PERFORMANCE OF A RECTANGULAR AIR INTAKE HAVING VARIABLE GEOMETRY COMPRESSION SURFACES AT MACH NUMBERS FROM 1.7 TO 2.5. Part II – The effect of incidence

Measurements have been made of the internal performance of a rectangular intake having variable geometry compression surfaces. The measurements have been made within a range of Mach numbers from 1.7 to 2.46 and at angles of incidence up to 10^{o}. The Reynolds number based on intake height was about 1.5×10^{6} for Mach numbers above 2 and 0.6×10^{6} for Mach numbers below 2. Some measurements at $M_{\infty} = 2.01$ were made at both Reynolds numbers.

The results confirm the findings of Part I of this Report that shock patterns can be used to predict accurately maximum mass flow and shock pressure recovery provided the assumption is made that the initial wedge angle is increased by just under one degree.

(Over)

ARC CP No.1242
December 1971

533.697.2 :
533.6.015 :
533.6.011.5

Brown, C. S.
Goldsmith, E. L.

MEASUREMENT OF THE INTERNAL PERFORMANCE OF A RECTANGULAR AIR INTAKE HAVING VARIABLE GEOMETRY COMPRESSION SURFACES AT MACH NUMBERS FROM 1.7 TO 2.5. Part II – The effect of incidence

Measurements have been made of the internal performance of a rectangular intake having variable geometry compression surfaces. The measurements have been made within a range of Mach numbers from 1.7 to 2.46 and at angles of incidence up to 10^{o}. The Reynolds number based on intake height was about 1.5×10^{6} for Mach numbers above 2 and 0.6×10^{6} for Mach numbers below 2. Some measurements at $M_{\infty} = 2.01$ were made at both Reynolds numbers.

The results confirm the findings of Part I of this Report that shock patterns can be used to predict accurately maximum mass flow and shock pressure recovery provided the assumption is made that the initial wedge angle is increased by just under one degree.

(Over)

These abstract cards are inserted in Technical Reports for the convenience of Librarians and others who need to maintain an Information Index.

Cut here

ARC CP No.1242
December 1971

533.697.2 :
533.6.015 :
533.6.011.5

Brown, C. S.
Goldsmith, E. L.

MEASUREMENT OF THE INTERNAL PERFORMANCE OF A RECTANGULAR AIR INTAKE HAVING VARIABLE GEOMETRY COMPRESSION SURFACES AT MACH NUMBERS FROM 1.7 TO 2.5. Part II – The effect of incidence

Measurements have been made of the internal performance of a rectangular intake having variable geometry compression surfaces. The measurements have been made within a range of Mach numbers from 1.7 to 2.46 and at angles of incidence up to 10^{o}. The Reynolds number based on intake height was about 1.5×10^{6} for Mach numbers above 2 and 0.6×10^{6} for Mach numbers below 2. Some measurements at $M_{\infty} = 2.01$ were made at both Reynolds numbers.

The results confirm the findings of Part I of this Report that shock patterns can be used to predict accurately maximum mass flow and shock pressure recovery provided the assumption is made that the initial wedge angle is increased by just under one degree.

(Over)

Cut here

DETACHABLE ABSTRACT CARDS

DETACHABLE ABSTRACT CARDS

The results also show that simple assumptions can be made as to the form of the shock pattern in order to extend these predictions into regions of shock detachment which arise inevitably when the intake is at large angles of incidence.

A simple correlation of losses other than shock losses with a 'turning loss' factor used in Part I, is found to serve equally well when the intake operates over a range of incidence from 0° to 10°.

The results also show that simple assumptions can be made as to the form of the shock pattern in order to extend these predictions into regions of shock detachment which arise inevitably when the intake is at large angles of incidence.

A simple correlation of losses other than shock losses with a 'turning loss' factor used in Part I, is found to serve equally well when the intake operates over a range of incidence from 0° to 10°.

The results also show that simple assumptions can be made as to the form of the shock pattern in order to extend these predictions into regions of shock detachment which arise inevitably when the intake is at large angles of incidence.

A simple correlation of losses other than shock losses with a 'turning loss' factor used in Part I, is found to serve equally well when the intake operates over a range of incidence from 0° to 10°.

The results also show that simple assumptions can be made as to the form of the shock pattern in order to extend these predictions into regions of shock detachment which arise inevitably when the intake is at large angles of incidence.

A simple correlation of losses other than shock losses with a 'turning loss' factor used in Part I, is found to serve equally well when the intake operates over a range of incidence from 0° to 10°.

Published by
HER MAJESTY'S STATIONERY OFFICE

To be purchased from
49 High Holborn, London WC1 V 6HB
13a Castle Street, Edinburgh EH2 3AR
109 St Mary Street, Cardiff CF1 1JW
Brazennose Street, Manchester M60 8AS
50 Fairfax Street, Bristol BS1 3DE
258 Broad Street, Birmingham B1 2HE
80 Chichester Street, Belfast BT1 4JY
or through booksellers

C.P. No. 1242

SBN 11 470800 2